2023

Use of Inner/Outer Sphere Terminology in Electrochemistry—A Hexacyanoferrate II/III Case Study

John Cassidy

Rafaela Cristina De Carvalho

Tony Betts

electrochem

MDPI

Review

Use of Inner/Outer Sphere Terminology in Electrochemistry—A Hexacyanoferrate II/III Case Study

John F. Cassidy [1,2,*], Rafaela C. de Carvalho [1,2] and Anthony J. Betts [1]

[1] Applied Electrochemistry Group, FOCAS Research Institute, Technological University Dublin, Central Quad, City Campus, Grangegorman Lower, DO7 ADY7 Dublin, Ireland; rafa_cdc@hotmail.com (R.C.d.C.); anthony.betts@tudublin.ie (A.J.B.)

[2] School of Chemical and BioPharmaceutical Sciences, Technological University Dublin, Central Quad, City Campus, Grangegorman Lower, D07 ADY7 Dublin, Ireland

* Correspondence: john.cassidy@tudublin.ie

Abstract: Salts of hexacyanoferrate II/III anions have been widely used as redox couple probe molecules to determine the characteristics of electrode surfaces. Examples include the assessment of electrocatalysts for energy applications and electrocatalysts for the detection of biological or chemical species, as well as the determination of electrochemically active surface areas. An examination of the electrochemical literature, based largely on cyclic voltammetric investigations, reveals a wide range of peak separation and/or heterogeneous electron transfer rate constants, classified sometimes as inner or outer sphere electron transfer processes. Originally developed for the mechanistic interpretation of inorganic transition metal compounds in solution, this terminology has since been extended to account for heterogeneous electron transfer occurring at electrodes. In the case of the hexacyanoferrate II/III anions, there can be a number of reasons why it sometimes behaves as an outer sphere probe and at other times displays inner sphere electron transfer characteristics. After examining some of the structural and chemical properties of the hexacyanoferrate II/III species, the methods used to determine such classifications are described. The most common method involves measuring peak-to-peak separation in a cyclic voltammogram to ascertain a heterogeneous rate constant, but it has inherent flaws. This paper reviews the reasons for the classification disparity, including the effects of various oxygen surface species, the influence of organic surface films, the nature of the cation counter-ion, surface adsorption and surface hydrophilicity/hydrophobicity. Other surface interactions may also take place, such as those occurring with Au corrosion or pH effects. These can impact the electrical double layer and thus may affect the electron transfer process. Consequently, it is recommended that hexacyanoferrate II/III should be considered a multi-sphere or alternatively a surface-sensitive electron transfer species.

Keywords: hexacyanoferrate II/III; ferrocyanide/ferricyanide; inner/outer sphere; multi-sphere electron transfer; cyclic voltammetry; Nicholson analysis; surface sensitive/insensitive

Citation: Cassidy, J.F.; de Carvalho, R.C.; Betts, A.J. Use of Inner/Outer Sphere Terminology in Electrochemistry—A Hexacyanoferrate II/III Case Study. *Electrochem* **2023**, *4*, 313–349. https://doi.org/10.3390/electrochem4030022

Academic Editor: Hsiu-Wei Cheng

Received: 24 May 2023
Revised: 24 June 2023
Accepted: 27 June 2023
Published: 11 July 2023

1. Introduction

The origin of the inner and outer sphere systems applied to redox events in homogeneous solutions is well-known [1]. Initially applied to homogeneous electron transfer reactions of octahedral transition metal complexes, significant contributions were made by the Nobel-Prize winners R A Marcus and H Taube, amongst others [2]. The outer sphere electron transfer (OSET) mechanism was invoked when two transition metal complexes in solution participating in an electron transfer (ET) reaction undergo ligand exchange reactions much more slowly than they participate in the ET process. In this case, the solvent coordination spheres are essentially maintained throughout the electron donor/acceptor electron transfer process. This OSET was the initial focus of the early Marcus ET theory [3–7]. In contrast, the inner sphere electron transfer (ISET) process frequently involves an exchange

of a ligand, along with the electron transfer. In this case, an ion or molecule in a bridged ligand donor/acceptor is generally involved in an intermediate state.

This terminology has also been applied to electron transfer processes occurring at electrode surfaces where it is referred to as a heterogeneous electron transfer (HET) reaction [3–6]. Normally, in the ISET case involving a transition metal complex, a central metal atom or a bridging molecule or ion or even a ligand in a reactant or product molecule is envisaged as being in intimate contact with the electrode surface. Electron transfer occurs directly between the reactant/product and the electrode surface [3,5,6]. ISET processes are frequently involved in redox reactions of technological importance, such as the reduction of hydrogen ions and the oxygen reduction reaction in hydrogen-based fuel cells, the reduction of copper ions in copper electrodeposition, the reduction of carbon dioxide and the oxidation of ammonia and oxidation of alcohols in direct alcohol fuel cells [3]. In contrast, OSET occurs when the ET takes place between a reactant molecule and an electrode surface through an intervening layer of solvent (the Inner Helmholtz Plane, IHP). The reactant or product species is therefore located outside the solvent layer immediately adjacent to an electrode surface. Electron transfer then occurs via a tunnelling process or an electron hopping process between the reactant or product, often depicted as being located in the Outer Helmholtz Plane (OHP) in the Electrical Double Layer (EDL) and the electrode surface adjacent to the IHP [3,5].

It is worthy of note, however, that the terms inner sphere (ISET) and outer sphere (OSET) are not universally adopted in the electrochemical literature. Although some electrochemistry textbooks use these terms [3–7], many others do not. The comparatively unusual nature of the OSET case is highlighted in a textbook by Schmickler and Santos who only mention two well-characterised OSET reactions in aqueous solutions; the Ruthenium II/III hexaammine trichloride and Fe II/III redox systems [6].

Weaver and Anson popularised the inner and outer sphere terminology by noting the effect of an added adsorbent anion in a redox reaction involving chromium ions [8,9]. In their view, in OSET processes, traditional electrochemical models apply as the rate-determining step is electron transfer (ET), which is usually interpreted by the Butler–Volmer approach, although sometimes more complex Marcus–Hush ET kinetic models have been considered. In the case of the inner sphere (ISET) mechanism, however, there could be a range of rate determining processes happening, such as slow kinetics of ligand exchange at the electrode surface, or possibly surface adsorption. This may lead to a different or even a mixed rate determining step [4].

In many electrochemical studies, well characterised OSET redox systems, such as those utilising ruthenium II/III hexaammine cations ($Ru(NH_3)_6^{2+/3+}$) in aqueous solutions or ferrocene ($Fc^{0/+}$) in non-aqueous solvents, can serve as valuable redox probes, especially in many electrochemical processes involved in the energy and environmental fields. An example is the determination of the electrochemically active (electro-active) surface area of an electrode, (ECSA or EASA), which requires fast electron transfer (i.e., a reversible process) and a redox system limited purely by diffusion control [10–12]. For a simple one-electron transfer process such as that involving hexacyanoferrate II/III anions commonly used approaches, include cyclic voltammetry (in conjunction with the Randles–Ševčík equation) and chronoamperometry (utilising the Cottrell equation). These can be adapted to determine the EASA, provided the diffusion coefficients of the reactants are accurately known [3,13]. For such OSET couples exhibiting fast heterogeneous electron transfer rates, there is generally little difference in the redox behaviour either before or after modification of the electrode surface. This lack of surface influence on the ET rate can thus be used as a criterion for the assignment of an OSET process. In general, however, there is a lack of criteria clearly defining or separating ISET from OSET in the literature.

In order to assess the efficacy of new electrode materials (such as 2D graphene or graphitic sp^2 nanomaterials) or modified electrodes (containing electrocatalysts), the hexacyanoferrate II/III redox couple has frequently been employed as a probe [14]. Potassium hexacyanoferrate (II/III), which is a single electron transfer couple may display quasi-

reversible behaviour indicative of a small heterogeneous rate constant. Often at an unmodified electrode such as those utilising carbon-based materials, the apparent heterogeneous rate constant could be slow (significantly less than 2×10^{-2} cm s^{-1} [3]). After surface modification or treatment, however, the rate generally increases, thus supporting the reason for the treatment of the electrode. This quasi-reversibility has attracted the use of the term inner sphere; characteristics of which are said to include the following:

(a) The electron transfer is often affected by the presence of oxygen and/or surface oxides or other carbon-oxygen species such as carbonyl groups or carboxylates/carboxylic acids (depending upon pH). Examples, including studies involving highly oriented pyrolytic graphite (HOPG), indicated that a greater quantity of edges in the electrode generally increased the apparent heterogeneous electron transfer, HET rate measured in terms of the rate constant, k^0 [15]. Smaller Graphene flakes also seemed to increase k^0 [16] In addition, a greater surface oxygen concentration in one study involving nanohorns also produced higher k^0 values [17]

(b) The electron transfer is frequently affected by pretreatment of the electrode. For example, exposure of HOPG to organic solvents caused a decrease in HET rate, k^0 [18], whereas laser scribing graphene had the opposite effect and enhanced the HET rate [19].

(c) The hexacyanoferrate II/III redox couple tends to adsorb on many electrode surfaces [20]. With continuous voltammetry the current for ferrocyanide oxidation decreases due to the occurrence of adsorption, prior to Prussian Blue formation [21] Another report described how adsorption of hexacyanoferrate was detected at a Pt ultramicroelectrode [22].

OSET systems are impervious to the three effects mentioned above and it is often considered that hexacyanoferrate II/III is an example of such a redox probe [23,24] For example, two articles published in the *Journal of Chemical Education* promulgated the notion that electron transfer in hexacyanoferrate is uniquely an OSET process [25,26]. This has led to some confusion, especially for those new to the field of electrochemistry. In practice, many articles in the electrochemical literature utilise two different types of redox couple probes, one classified as an "inner sphere" (ISET) probe and the other an "outer sphere" (OSET) probe such in order to identify such effects [3–5]. It is interesting to note that hexacyanoferrate II/III redox probes have been ascribed to both categories over the years as outlined below.

The aim of this article is to call into question whether the ISET/OSET mechanism terminology should be employed for such heterogeneous electron transfer reactions, especially those involving hexacyanoferrate II/III ions, as the use of the terms ISET/OSET merely causes confusion. An investigation of the literature was conducted, with suggestions that the heterogeneous electrochemical surface reactions involving the hexacyanoferrate II/III redox species may utilise either ISET or OSET processes, depending on the conditions employed in the electrochemical study being undertaken. This makes a definitive assignment of hexacyanoferrate II/III redox species to either an ISET or an OSET problematic in practice. The novelty behind this review is the presentation of evidence currently scattered throughout the literature, which will be of benefit to experienced electrochemists and at the same time will provide guidance for less experienced electrochemists. Careful consideration should be given to the continued use of the ISET/OSET classification system when reporting electrochemical results utilising hexacyanoferrate II/III redox species. A new alternative classification system for future use with this often-used redox species is recommended for adoption in this paper.

2. Hexacyanoferrate II/III Redox Probes

Figure 1 shows a cyclic voltammogram (CV) initially involving potassium hexacyanoferrate II oxidation in 0.1 M KCl supporting electrolyte, followed by potassium hexacyanoferrate III reduction on the reverse scan, conducted on a vacuum heat-treated commercial screen-printed carbon electrode (SPCE) [27]. It can be seen that the peak-to-peak separation

(peak separation) value, ΔE_p of 400 mV is much greater than the ideal value of 57/n mV to 60.5/n mV, predicted theoretically for a reversible single electron transfer reaction (i.e., 57 mV–60.5 mV, with n = 1) [3]. It should be noted that the ΔE_p value obtained when conducting such a cyclic voltammetric investigation depends upon the upper reverse potential employed with the limit being 57/n mV, although in practice it is typically 58/n or 59/n mV at 25 °C. The ΔE_p apparent in Figure 1 is indicative of a very slow HET rate (i.e., a very small k^0 value, certainly much less than 0.02 cm s^{-1}). According to the well-known Matsuda and Ayabe criteria, assuming a diffusion coefficient D of approximately 10^{-5} cm^2 s^{-1} and with typical scan rates, v ranging between 0.02 V/s and 1.0 V/s, reversible kinetics yields k^0 values above about 0.04–0.3 cm s^{-1} [3]. It should be noted that this approach to the determination of k^0 is dependent upon the factor $0.3v^{1/2}$, which is clearly a function of the scan rate measured in V/s [3,4]. On the other hand, quasi-reversible kinetics measured in this scan rate range generally possess k^0 values of between about 2.8×10^{-6} and 4.2×10^{-2} cm s^{-1}. For this range of scan rates, irreversible kinetics are indicated by very small values of k^0, less than approximately 8.5×10^{-7} to 2.8×10^{-6} cm s^{-1}. For the hexacyanoferrate II/III redox couple, a k^0 value of 0.1 cm s^{-1} is listed for the HET k^0 value. This is in the reversible kinetics range, although the electrolyte and electrode are not given [5].

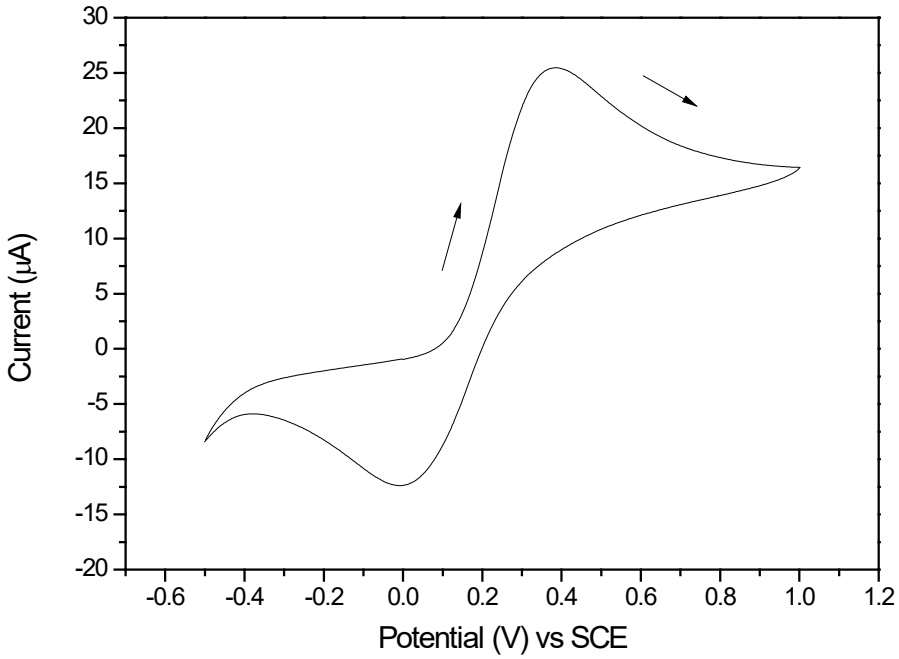

Figure 1. Cyclic voltammogram recorded in 5 mM potassium ferrocyanide in aerated 0.1 M KCl supporting electrolyte at a vacuum heat-treated screen-printed carbon electrode (SPCE) obtained at a scan rate of 0.05 Vs^{-1}. The counter electrode was carbon ink and an external saturated calomel electrode served as a reference electrode [27].

Large peak separations for what is notionally an OSET redox probe (hexacyanoferrate II/III) such as that displayed in Figure 1, may be due to a combination of factors. The small heterogeneous rate constant, k^0 may be due to adsorption or de-solvation effects at the electrode surface [3,28]. Often this may occur in combination with other effects, such as high inherent internal resistance within the electrode material (such as a carbon paste or a screen-printed carbon electrode) and/or the presence of uncompensated solution resistance. Similar effects have been observed by others on screen-printed carbon electrodes SPCE [29,30]. Furthermore, in Figure 1, the i_{pa}/i_{pc} peak ratio is evidently not 1.0 (i.e., it is most likely <1.0 even after background correction), which is indicative of adsorption of the reduced species $Fe(CN)_6^{4-}$. It is thus clearly not a reversible cyclic voltammogram but instead typifies a quasi-reversible system. It should also be noted that the first portion of the CV curve displayed in Figure 1 near −0.5 V (vs Ag/AgCl) shows a significant cathodic cur-

rent, possibly due to the occurrence of the oxygen reduction reaction (ORR) in this aerated electrolyte, where the formation of hydroxide and/or other oxygen-containing species (e.g., superoxide anion) invariably happens, effectively modifying the SPCE electrode surface.

In contrast, Figure 2 (left-hand side), taken from the literature shows a near-ideally reversible CV behaviour, with a ΔE_p of nearly 60 mV and a peak cathodic/anodic current (i_{pc}/i_{pa}) ratio of approximately 1.0. [31]. In this example, a surface treatment was applied to a carbon electrode (termed a GUITAR electrode, with the acronym representing a pseudo-graphite nanocrystalline graphite-like hydrogenated amorphous carbon comprising 85% sp^2 and 15% sp^3 carbons). On ageing in air, however, a HOPG electrode (whose CV is presented on the right-hand side of Figure 2) shows a much wider peak separation value ΔE_p of 221 mV, which indicates that the HOPG electrode is not stable in air and a time-dependent behaviour occurs.

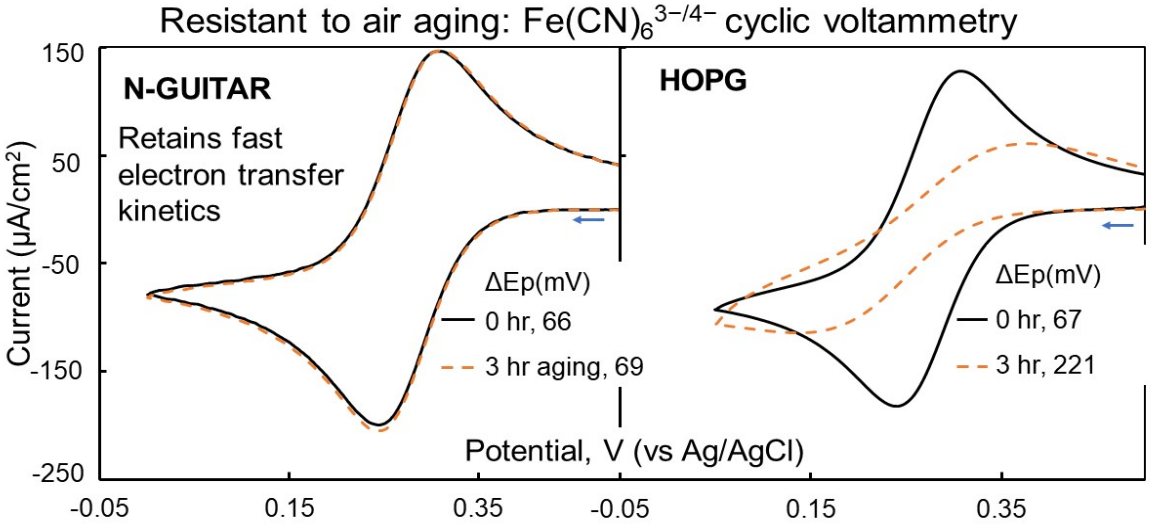

Figure 2. Cyclic voltammograms obtained for the one electron reduction of ferricyanide ions in aerated 0.1 M KCl at 50 mV/s in N-doped amorphous carbon (**left**) and (**right**) in Highly Oriented Pyrolytic Graphite (HOPG) showing a range of ΔE_p values [31].

The examples presented in Figures 1 and 2 show the wide variation in the electrochemical behaviour of the hexacyanoferrate II/III redox system determined by cyclic voltammetry where the following redox couple occurs: [32]

$$[Fe(CN)_6]^{3-} + e^- \rightleftharpoons [Fe(CN)_6]^{4-} \qquad E^{0'} = 0.3610 \pm 0.0005 \text{ V (NHE)} \tag{1}$$

No bonds are either broken or formed in this simple one ET reaction, so it is a useful model reaction for the investigation of electrode surfaces. The central iron in each anion undergoes minimal change in radius as a result of this redox couple reaction (radii are 61 pm for Fe^{2+} and 55 pm for Fe^{3+} in these transition metal octahedral compounds, respectively) [33].

Potassium hexacyanoferrate II/III (also referred to as potassium ferrocyanide/potassium ferricyanide and with an IUPAC name of potassium hexacyanidoferrate II/III) is frequently employed as a standard couple or probe in electrochemical investigations. The two oxidation states of the redox couple are thought to be stable and the compounds are inexpensive, relatively non-toxic, water-soluble, and readily accessible. Consequently, they are widely used in research and undergraduate laboratories.

Both hexacyanoferrate II/III have similar chemical structures, which accounts for their physical and electrochemical characteristics. The hexacyanoferrate II or ferrocyanide anion ($[Fe(CN)_6^{4-}]$) contains a central Fe^{2+} cation in a low spin d^6 configuration bound singlet ground state (S = 0) with 6 strongly stabilised cyanide ions in an octahedral configuration (O_h molecular structure). It has an electronic configuration of:

$$1s(a_{1g})^2 2p(t_{1u})^6(\sigma(e_g))^4(3d(t_{2g}))^6(\sigma_{CN}{}^*(e_g))^0(\pi_{CN}{}^*(t_{2g}))^0$$

Comprising 6 electrons in three 3d orbitals, labelled t_{2g} [34–36]. These paired spins mean that the hexacyanoferrate II anion, as commonly found in potassium hexacyanoferrate II, is diamagnetic. Like most transition metal complexes containing ligands with π-bonds, ligand–metal bonding consists of both σ-donation and π-back-donation within the valence band. The former emanates from the mixing of the occupied ligand and partly occupied or unoccupied metal orbitals resulting in electron density redistribution from ligand to metal. The π back-donation arises from electronic mixing between the occupied orbitals of the metal and the ligand's unoccupied orbitals. Specifically in this compound, the electronic charge is transferred from the highest occupied lone pair orbitals of the CN^- to the empty Fe^{2+} σ*(e_g) orbitals, whilst in π-back-donation, Fe^{2+} 3d(t_{2g}) electrons are moved into the lowest unoccupied antibonding π* ligand orbitals.

For the other redox partner, hexacyanoferrate III (ferricyanide anion, $[Fe(CN)_6]^{3-}$) the σ-donation is strengthened slightly, while the π back-donation is diminished [35]. Also containing a central iron cation (Fe^{3+}), this anion exists in a low spin d^5 configuration (S = 1/2) with five electrons in three degenerate t_{2g} orbitals resulting in a weak Jahn–Teller distortion to D_{4h} symmetry [36]. It is also paramagnetic and has a weaker ligand field stabilisation energy than its hexacyanoferrate II counterpart [37]. With a similar electronic structure, it has one less d orbital electron in the three 3d orbitals, labelled $(t_{2g})^5$. Consequently, it would be expected to display similar bonding characteristics. In fact, cyano ligands are amongst the strongest identified in the spectrochemical series [38].

The oxidation of hexacyanoferrate II to hexacyanoferrate III species and the reverse reduction reaction (formation of hexacyanoferrate II from hexacyanoferrate III), described in Equation (1) above, does not seem to involve large structural changes [4,6]. This is borne out by a small change in the Fe-C bond length of 2.6 pm, which was reported on reduction of $[Fe(CN)_6{}^{3-}]$ to $[Fe(CN)_6{}^{4-}]$ indicative of a small Jahn–Teller distortion effect (Fe-C being 191.3 pm in $Fe(CN)_6{}^{4-}$ and for $Fe(CN)_6{}^{3-}$ four Fe-C bonds of 191.6 pm with two being 193.9 pm in length) [39]. The bond angles are invariant (117.9°) [40]. There are, however, subtle differences between the two anions in water [41]. Both molecular dynamic MD computational and 2D IR experimental results indicated that the frequency correlation function relaxes more slowly in the case of the ferrocyanide ion, probably due to stronger hydrogen bonding occurring in this more highly charged anion (4-), which is probably kosmotropic. This is manifest in the small differences in the diffusion coefficients exhibited by the two anions; with D_0 of 7.2×10^{-6} cm^2/s for the hexacyanoferrate III anion whilst there is a lower D_R of 6.4×10^{-6} cm^2/s for the hexacyanoferrate II anion [42]

Potassium hexacyanoferrate III and its hexacyanoferrate II counterpart are precursors to the formation of Prussian Blue (PB, $K[Fe^{III}[Fe^{II}(CN)_6])$, an intensely blue-coloured pigment used in paints and once used in the creation of blueprints. This complex compound forms in the presence of ferric ions and hexacyanoferrate II salts, respectively, or with ferrous ions and hexacyanoferrate III salts [43]. During storage in aerated conditions, aqueous solutions of hexacyanoferrate II can degrade over time and they are also known to be unstable in light [44]. Thus, care should be taken to ensure that long-term exposure to both oxygen and light is kept to a minimum when preparing aqueous solutions comprising these compounds for carrying out electrochemical investigations.

Table 1 gives some examples of the peak separation values ΔE_p and the heterogeneous rate constants k^0 both of which show wide variation in values using the ferro/ferricyanide redox probe. Inspection of this table reveals the use of a diverse set of electrode surfaces, supporting electrolytes and the presence (or absence) of oxygen in these studies. It should be emphasised that this is by no means a comprehensive listing, but it clearly demonstrates that there exists a wide range of both ΔE_p and k^0 values reported in the literature for the hexacyanoferrate II/III couple.

Table 1. Table of a variety of electrode materials at which hexacyanoferrate II/III was employed as a model redox probe where k^0 is the apparent heterogeneous rate constant in cm s^{-1} and ΔE_p is the peak-to-peak separation in mV. The various authors assign the mechanism to be inner sphere (ISET) or outer sphere (OSET).

Electrode Material	Year	Assignment	Attributes k^0 cm/s and ΔE_p/mV	Deoxy-Genated *	Supporting Electrolyte/ Scan Rate	Reference
Nanosized graphite sheets in a carbon film	2018	Inner	$k^0 = 0.026–0.09$ $71 < \Delta E_p < 145$	Yes	1 M KCl 0.1 V/s	[15]
Boron doped carbon electrodes (500–8000 ppm)	2017	Inner	$k^0 = 3.75 \times 10^{-5}$– 2.07×10^{-2} $59 < \Delta E_p < 87$	No	1 M KCl 0.025–0.3 V/s	[45]
Au nanocatalyst on ITO	2016	Outer	---	No	PBS pH 7.4 0.02 V/s	[46]
Reduced graphene oxide/Nafion composite	2019	Outer	$28 < \Delta E_p < 133$	Yes	0.1M KCl 0.1–0.4 V/s	[47]
HOPG with droplet cell configuration	2015	Outer	$k^0 > 0.46 \pm 0.03$	No	0.1 M KCl 2–10 V/s	[48]
Graphite and graphene flakes with different flake sizes in nujol	2018	Inner	$k^0 = 6.04 \times 10^{-5}$– 1.93×10^{-3} $105 < \Delta E_p < 833$	Yes	0.1 M KCl 0.1 V/s	[16]
Thin graphene layer on Au	2016	Outer	$k^0 =$ 4×10^{-4}–1.4×10^{-2}	No	0.1 M KNO_3 0.1 V/s	[23]
Single walled nanohorns	2019	Inner	$k^0 = 5.59 \times 10^{-2}$ $\Delta E_p = 71$	Yes	0.1 M KCl 0.25–0.3 V/s	[17]
BDD	2004	Outer	$k^0 = 2 \times 10^{-5}$–4×10^{-4} $930 < \Delta E_p < 1420$	No	0.5 M H_2SO_4 0.1 V/s	[49]
Diamond graphite composite	2003	Outer	$120 < \Delta E_p < 430$	No	0.5 M H_2SO_4 0.1 V/s	[24]
BDD	1999	Inner	$70 < \Delta E_p < 198$	Yes	1 M KCl and 50 mM phosphate Buffer pH 7.2 0.1 V/s	[50]
Pt ultramicro-electrodes	2002	---	adsorbed hexacyanoferrate-steady state voltammetry	Yes	0.1 M KCl 0.01 V/s	[22]
Carbon silicon films	2017	Inner	$k^0 = 5.4 \times 10^{-3}$	No	0.1 M KCl 0.05 V/s	[51]
Carbon black/ chitosan composite	2015	Inner	$63.4 < \Delta E_p < 452$	No	0.1 M KCl 0.05 V/s	[52]
Pt nanofluidic recycling cell	2014	Outer	Based on power spectral density data, Hexammine Ru(III) adsorbed more than hexacyano-ferrate III	No	-	[20]
Laser scribed graphene	2014	Inner	$k^0 = 2.373 \times 10^{-2}$ to 3.3×10^{-4} $59 < \Delta E_p < 176$	No	0 M KCl 0.01 V/s	[19]
Pencil Graphite Electrode	2012	-	$75 < \Delta E_p < 741$	Yes	1 M KCl 0.1 V/s	[53]
GC, PGE, HOPG	2010	-	$80 < \Delta E_p < 220$	Yes	0 M KCl 0.1 V/s	[54]
BDD, GC, SPCE	2003	-	$k^0 = 1.67 \times 10^{-5}$ -5.5×10^{-2}	No	1 M KCl	[29]
HOPG with oxygenated edge planes	2006	Inner	Basal plane $227 < \Delta E_p < 596$ Edge plane $89 < \Delta E_p < 137$	Yes	0.1 M KCl 0.1 V/s	[55]

Table 1. *Cont.*

Electrode Material	Year	Assignment	Attributes k^0 cm/s and ΔE_p/mV	Deoxy-Genated *	Supporting Electrolyte/ Scan Rate	Reference
Basal plane HOPG with 10–20% Edge planes	2011	Inner	Organic solvent affects k^0 = ~0.02 (without MeCN), 4×10^{-5} (NaCl), 4×10^{-6} (KCl) 8.5×10^{-3} (CsCl)	Yes	0.1 M salts (NaCl, KCl, CsCl) 0.1 V/s	[18]
Nanotubes on carbon screen printed electrodes	2014	Inner	Graphite k^0 = 5.76×10^{-3} SWCNT k^0 = 10.7×10^{-3} MWCNT k^0 = 7.5×10^{-3}	Yes	0.1 M KCl 0.05–0.1 V/s	[56]
GC Electrodes with lipid layers	2002	Outer	-	No	20 mM $NaNO_3$ and 3 mM $CaCl_2$ 0.1 V/s	[57]
SWCNT on GC	2008	-	Thin layer behaviour	No	0.1 M KCl 0.01–0.7 V/s	[58]
Graphene paste Graphite paste	2013	Inner	ΔE_p = 153.8 ΔE_p = 393.1	Yes	0.1 M KCl 0.1 V/s	[59]
Laser scribed graphene on chip	2016	Inner	k^0 = 0.115 (LSG) k^0 = 0.282 (Pt/LSG) ΔE_p = 86 (LSG) ΔE_p = 71 Pt LSG)	No	0.1 M KCl 0.05–0.15V/s	[60]
Inkjet carbon-graphite ink	2008	Outer	ΔE_p = 136 ± 14 (Direct Write) k^0 = 2.4×10^{-3} ΔE_p = 153 ± 8 (Screen Printed) k^0 = 1.9×10^{-3}	No	1 M KCl 0.01–0.1 V/s	[61]
Boron doped carbon	2002	Inner	ΔE_p = 673–716	No	0 M KCl 0.1 V/s	[62]
Graphene on Au coated Si (SECM)	2016	Outer	k^0 = 4.0×10^{-4}– 1.4×10^{-2}	No	0.1 MKNO_3 0.1 V/s	[23]
HOPG (EPPG/BPPG) Graphene Graphite	2011	Inner	ΔE_p = 60 (EPPG) ΔE_p = 242 (BPPG) ΔE_p = 192 (HOPG /graphene) ΔE_p = 66 (HOPG/Graphite)	No	1 M KCl 0.1 V/s	[63]
Graphene	2017	Inner	ΔE_p = 400–900	No	0.1 M KNO_3 0.025 V/s	[64]
N-doped Pyrolytic Carbon	2013	Inner	ΔE_p = 71.7 k^0 = 4.4×10^{-2}	Yes	1 M KCl 0.1 V/s	[65]
Pyrolytic Carbon	2010	-	ΔE_p = 80 k^0 = 1.3×10^{-2}	Yes	1 M KCl 0.1 V/s	[66]
HOPG and Graphene	2010	Outer	ΔE_p = 67 (HOPG edge plane) ΔE_p = 238 (HOPG basal plane) ΔE_p = 122 (HOPG + Graphene)	No	1 M KCl 0.1 V/s	[67]
Diamond/graphite	2003	Outer	120 < ΔE_p430	No	0.5 M H_2SO_4 0.1 V/s	[24]
SPCE	2009	Outer	98 < ΔE_p < 466	No	1 M KCl 0.1 V/s	[30]
Screen Printed SWCNT	2013	Outer	k^0 = 1.1×10^{-3} (SPCE) k^0 = 1.4×10^{-3} (with SWCNT)	No	0.1 M KCl 0.01–0.4 V/s	[68]

Table 1. *Cont.*

Electrode Material	Year	Assignment	Attributes k^0 cm/s and ΔE_p/mV	Deoxy-Genated *	Supporting Electrolyte/ Scan Rate	Reference
Q-graphene	2012	Inner	$68 < \Delta E_p < 432$ $4.66 \times 10^{-3} < k^0 < 1.86 \times 10^{-2}$	Yes	1 M KCl 0.05 V/s	[69]
Multilayer graphene, BPPG, EPPG	2014	Inner	-	Yes	1 M KCl 0.05 V/s	[70]
Graphene	2014	Inner	$98 < \Delta E_p < 190$ (EPPG and BPPG) $\Delta E_p = 1148$ (m-Graphene) $\Delta E_p = 1243$ (q-Graphene)	Yes	0.1 M KCl 0.1 V/s	[71]
BDD and amide and carboxyl Graphene nanoflakes	2014	-	$\Delta E_p = 65$ (BDD) $109 < \Delta E_p < 250$ (c-GNF) $\Delta E_p = 70$ (a-GNF)	Yes	0.01–1.0 M KCl and 0.1 M K_2HPO_4 0.05 V/s	[72]
PGE	2008	-	$\Delta E_p = 90$–450	Yes	1 M KCl 0.1 V/s	[73]
Iridium	1999	-	$\Delta E_p = 74.4$ $k^0 = 7.2 \times 10^{-2}$	No	1 M KNO_3 3.5 V/s	[74]
Pt and GC	2013	Outer	$\Delta E_p = 66$ (Pt), $\Delta E_p = 86$ (GC) $k^0 = 4.1 \times 10^{-2}$(Pt) $k^0 = 1.2 \times 10^{-2}$ (GC)	No	1.0 M KCl 0.2 V/s	[26]
GC	2014	-	$87 < \Delta E_p < 172$ $k^0 = 5 \times 10^{-3}$ to 8×10^{-3}	No	1.0 M KCl 0.89–1.0 V/s	[75]
Pt	2022	-	$71 < \Delta E_p < 135$ 1 mM–100 mM $Fe(CN)_6^{3-}/Fe(CN)_6^{4-}$	No	0.1 M K_2SO_4 0.01 V/s	[76]

Note: GC = Glassy Carbon, PGE = Pencil Graphite Electrode, HOPG = Highly Oriented Pyrolytic Graphite, SWCNT = Single Walled Carbon Nanotube, ITO = Indium Tin Oxide, BDD = Boron Doped Diamond, SPCE = Screen Printed Carbon Electrode, PBS = Phosphate Buffer Solution, MeCN = acetonitrile, EPPG = Edge Plane Pyrolytic Graphite. * Unless deoxygenation was explicitly described in the paper, it was assumed not to have been performed.

Further examples listing a similarly disparate range of heterogeneous rate constant values are also given in papers by Huang et al. [77] and Unwin et al. [78]. From Table 1, it can be seen that for some cases designated as outer sphere, (OSET) the values for k^0 are quite small with ΔE_p typically larger than the 57–62 mV range for a near-reversible electron transfer process. This implies that the hexacyanoferrate II/III system is quite often a quasi-reversible one in view of the slow HET rates. Poor repeatability (i.e., inherent variation between results obtained from carrying out the same experiment repeatedly) and poor reproducibility, with significant variations reported for the same electrode materials, are however problematic. As a result, other redox probes are now more often favoured [10,78].

Table 1 illustrates the extent of confusion regarding the hexacyanoferrate II/III system in the literature. In some cases, oxygen was removed from the electrolyte, generally yielding lower ΔE_p values and simultaneously faster HET rate constants k^0. While the range of potentials scanned in a cyclic voltammogram may not extend to allow oxygen reduction, it is still possible that the presence of oxygen may affect the redox couple and/or the electrode surface, as illustrated in Figure 1. This is especially true with carbon surfaces, through the formation of various carbon-oxygen species, or with the occurrence of surface-adsorbed oxygen [14,29,78]. Such species can either electrostatically repel hexacyanoferrate II/III anions ($[Fe(CN)_6]^{3-}/[Fe(CN)_6]^{4-}$) or may block access to the electrode surface. In contrast, negatively charged carbon-oxygen functional groups can attract positively charged redox probes, such as ruthenium II/III hexaammine trichloride, a commonly used OSET redox

probe. In fact, the presence of oxygen is known to affect the voltammetry of ferrocene carboxylate for example [79] as well as that of the hexacyanoferrate II/III couple [50,55].

One problem frequently encountered with the designation of an ISET or OSET process is the lack of clarity on the experimental classification approach undertaken in the work. In some early work conducted on various chromium aquo and chromium ammino complexes the logarithm of the apparent measured rate constant k_{app} (at a known bulk concentration C^b where $k_{app} = i/FC^b$) vs. potential, E yielded straight line plots over two decades [8,9]. These studies were conducted in deaerated sodium perchlorate electrolytes on hanging mercury drop electrodes. When used together with iodide anions, which are known to adsorb onto mercury electrode surfaces, this was suggested as a method for distinguishing between an ISET or an OSET process. In the presence of iodide anions, distinct deviations from the linear log k_{app} vs. E plots occurred; trending upwards in the case of an OSET and downwards in the ISET system. In the OSET case, this was ascribed to Coulombic enhancement of the reactant concentration in the Outer Helmholtz Plane (OHP) of the Electrical Double Layer (EDL), for fluoro, sulphate and aquo ligands. For the ISET case however, involving chloro, bromo, azido, nitrate and thiocyanate ligands, an additional unspecified kinetic factor (possibly an adsorption effect) was implicated. In addition, the measured transfer coefficient α, obtained from a Tafel plot analysis, was higher in the OSET case (between 0.56 and 0.58) and lower in the ISET case (ranging from 0.35 to 0.43). It should be pointed out though, that this experimental classification was for a very different series of transition metal complexes than the hexacyanoferrate II/III case and mercury was used as the electrode, whose behaviour can be different from other electrodes, such as those based on carbon.

Transfer coefficients arising from Tafel slope analysis conducted on Au and Pt electrodes using hexacyanoferrate III anions were reported by Torres [25]. A reduction transfer coefficient α_{red} of 0.606 on Au and a hexacyanoferrate II oxidation transfer coefficient β_{ox} of 0.378 (combining to yield a transfer coefficient sum of 1.084, quite near the expected value of 1.0 for a simple one electron transfer). Experiments were conducted in a deoxygenated 1 M $NaNO_3$ electrolyte on a Au rotating disk electrode (RDE) operating at 2500 rpm, at a slow sweep rate of 3 mV/s. Similarly on a Pt RDE electrode, α_{red} was determined to be 0.631 and β_{ox} was 0.363 (with a combined total of 0.994). Furthermore, both electrodes displayed similar exchange current density i^0 values (201 μAcm^{-2} on Au and 266 μAcm^{-2} on Pt), indicative of very little interaction with the electrode surface. Relatively small peak separation (ΔE_p) values of 66 mV were obtained from CV curves on Au electrodes and a similar ΔE_p of 65 mV was found on Pt electrodes under identical conditions, demonstrating relatively fast near-reversible kinetics in both these conditions. This behaviour was assigned to an OSET process. Comparison with another redox probe system (Fe(III)/Fe(II) in 1 M H_2SO_4) indicated very different behaviour. Markedly lower α_{red} values were found (0.27 and 0.34 for Au and Pt, respectively) along with very different i^0 values of 6 μAcm^{-2} for Au and 100 μAcm^{-2} for Pt. Together with large peak separation ΔE_p values of 426 mV and 126 mV, this latter redox couple was considered to be an ISET process, rather than an OSET system.

Analyses based on Butler–Volmer kinetics, such as the determination of Tafel slopes and thereby transfer coefficients are not, however, thought to be appropriate for ISET processes, as linear plots are invariably difficult to obtain for these ET systems [3,6]. In fact, a curved Tafel plot is presented in the textbook by Albery for the hexacyanoferrate II/III redox couple quoting data reported by Frumkin et al. on Hg and thallium amalgam electrodes [80].

The commonly held view is that OSET processes are most often considered to be fast ET processes with inherently fast kinetics (high k^0 values) [25,26]. Here, it is assumed that the redox molecules come sufficiently near the electrode surface for electrons to hop or tunnel across a monolayer of solvent (the IHP of the EDL), but the ionic species (hexacyanoferrate II/III) do not directly interact with the electrode surface itself. In such OSET situations, redox probes are thought to be influenced only by the electronic structure of the electrode

surface. For ISET processes, however, inner-sphere probes are influenced not only by the electrode's electronic structure but also by the surface itself, which can interact with the reactant, intermediate, and/or product. For the ISET case surface functional groups, adsorption sites, and defects can all affect the surface chemistry and may inhibit the ET process, resulting in diminished HET k^0 values [10].

With this in mind, the designation of an ISET or an OSET process is sometimes based on a Nicholson analysis, which is frequently conducted for quasi-reversible ET reactions with peak separations larger than about 62 mV, but invariably less than 212 mV [81]. By adjusting a cyclic voltammogram's scan rate, it may be feasible to estimate the redox reaction's kinetics, moving it from a region where the Nicholson analysis is not appropriate to one in which the kinetics then fall into the quasi-reversible domain and thus become amenable to this analysis [26]. The Nicholson approach enables the determination of HET rates (k^0 values) through the experimental measurement of ΔE_p from cyclic voltammograms in conjunction with the expression:

$$\psi = k^0[(\pi D_O n v F)/(RT)]^{-1/2}\left(\frac{D_R}{D_O}\right)^{-\alpha/2} \quad (2)$$

where ψ is a kinetic parameter tabulated by Nicholson, D_O is the diffusion coefficient of the hexacyanoferrate III anion (7.2×10^{-6} cm^2/s) D_R the diffusion coefficient for the hexacyanoferrate II anion (6.4×10^{-6} cm^2/s) [42], n is the number of electrons transferred (1 for hexacyanoferrate II/III), v is the scan rate (in V/s) and π, F, R, and T all have their usual meanings. The transfer coefficient α is usually taken to be 0.5. This equation predicts that the peak separation value ΔE_p will increase with the scan rate. Equation (2) can then be simplified for the hexacyanoferrate II/III by using the values of D_O and D_R to yield the expression

$$\psi = k^0[(\pi D_O v F)/(RT)]^{-1/2}(1.030) \quad (3)$$

Lavagnini et al. plotted the Nicholson tabulated data and developed the following equation relating the peak separation ΔE_p value measured in a CV curve to the kinetic parameter ψ as follows [82]:

$$\psi = \left[-0.6288 + 0.0021\left(\Delta E_p\right)\right]/\left[1 - 0.017\left(\Delta E_p\right)\right] \quad (4)$$

Another equation relating $ln\ \psi$ to the $ln\ \Delta E_p$, was also proposed by Swaddle [83]

$$ln\psi = 3.69 - 1.161ln\left(\Delta E_p - 59\right) \quad (5)$$

By either measuring a value of ψ from the plotted curve of Nicholson's tabulation and using Equation (1), or by plotting ψ versus $v^{-1/2}$ the slope $[(\pi D_O F)/(RT)]^{-1/2}\left(\frac{D_R}{D_O}\right)^{-\alpha/2}$ for a number of scan rates v in conjunction with Equation (2), k^0 may be determined.

For very low values of k^0 when ΔE_p exceeds 212 mV, Lavagnini et al. developed an extended equation for the direct determination of the HET rate constant [82]

$$k^0 = [2.18(\alpha D\pi nF/RT)^{\frac{1}{2}}]\exp[-\left(\frac{\alpha^2 nF}{RT}\right).\Delta E_p] \quad (6)$$

There are, however, a number of problems with this approach [84,85]. Although uncompensated resistance R_u can be accounted for by using potential feedback and/or a Luggin probe for the reference electrode, often this is not carried out in practice thereby influencing the currents/potentials measured. Another contribution not always accounted for by many using the Nicholson approach is the non-faradaic current due to capacitance C_{dl} arising from electrical double-layer charging. This is especially true at faster scan rates, such as 0.1 V/s. Like the R_u, it can be accounted for experimentally, in this case by conducting a separate experiment under identical conditions with the hexacyanoferrate II/III species absent. The background current may then be determined and subtracted from a comparable experiment carried out in the presence of the hexacyanoferrate II/III

species. Like the R_u compensation adjustment, this is, however, not always carried out in many studies.

Another effect arises from variations in values of the transfer coefficient α, used in both the Butler–Volmer and the Marcus–Hush electrode kinetics approaches, which may deviate from 0.5 as discussed earlier [6,86]. An accurate assessment of the formal potential E^0 is also required in order to account for variations between experimental runs. Ultimately these factors can cause significant changes in the values of k^0 obtained by the Nicholson analysis. More accurate values can be determined by using computer simulations in packages including DigiSim, KISSA, COMSOL Multiphysics, DigiElch, and MECSim to obtain the best-fit curves and thus determine accurate values for each parameter (C_{dl}, R_u, E^0, α, and hence k^0) [87]. Most of these models are based on Butler–Volmer kinetics, although Marcus–Hush theory which takes into account the dynamics and solvent re-organisation of the ET process may further enhance this modelling approach in some cases [3,5,6].

While the majority of authors in Table 1 assign the ISET regime to the hexacyanoferrate II/III couple, others attribute the behaviour to the OSET mechanism. The assignment of the OSET is quite often promulgated in the literature, including the two articles referred to previously, which were both published in a popular journal for novice electrochemists [25,26]. Typically, OSET is most often associated with the display of near-reversible voltammetry (i.e., small ΔE_p near 60 mV) exhibiting relatively fast k^0 values, whereas ISET generally involves much slower quasi-reversible kinetics. It seems that some researchers may have been unaware of this distinction and instead based their classification on the presumption of OSET from the literature, without specific reference to their own results. Even though Table 1 is by no means a comprehensive listing, it does highlight the variation in the assignment of ISET or OSET in the literature to the hexacyanoferrate II/III redox couple and the variability of both ΔE_p and k^0 results for this commonly used redox couple system.

This is an illustration of the "pathologicaly variable" hexacyanoferrate II/III redox system, with quasi-reversible ET behaviour being representative of slower HET kinetics [87]. Bond et al. confirmed this by carrying out a series of repeated measurements of the electrode kinetics of the hexacyanoferrate II/III redox system on a freshly prepared glassy carbon (GC) electrode using an ac voltammetry method [87]. In spite of meticulous electrode preparation involving careful polishing and a rigorous cleaning routine performed between ten repeated experiments, a wide variation in the HET rate was reported. Meticulous analysis was carried out by performing 10 separate experiments on a carefully cleaned GC electrode surface. The extent of the variation is presented in Table 2. These experiments were conducted in a deaerated 3 M KCl electrolyte with a Luggin capillary and a Ag/AgCl (3 M) reference electrode. It was found that k^0 values on the same GC sample ranged between 5.5×10^{-3} cm s^{-1} and 1.9×10^{-2} cm s^{-1} representing a nearly four-fold difference. Results from a similar study performed by the same group are also listed in Table 2 [88].

Table 2. Parameters obtained from a series of 10 experiments using ac voltammetry in conjunction with sophisticated modelling methods in the hexacyanoferrate III reduction reaction [87,88].

	k^0/cm s^{-1}	α	E^0/mV (*NHE*)	R_u/Ω	Reference
Range (N = 10)	0.0055–0.019	0.50–0.54	417–423	4–8	[87]
Average (Range)	0.010 (0.002-0.018)	0.52	420	15.2	[88]

These results were ascribed to the occurrence of an ISET system for the hexacyanoferrate II/III couple in preference to an OSET process on the GC electrodes. This "pathologically variable" redox couple involves ET on a heterogeneous GC electrode surface comprising microscopically different regions, which are sufficiently near each other to approximate mass transport by planar diffusion (i.e., with overlapping diffusion layers), resulting in quasi-reversible electrode kinetic behaviour. In order to overcome these issues, Bond et al. later adopted a more stringent approach through the use of ac voltammetry in conjunction with advanced computer modelling techniques involving Bayesian statis-

tics [89,90]. Relationships between the parameters typically used to classify the ISET or OSET processes were investigated using a Butler–Volmer ET model.

As described earlier HET reactions displaying irreversible kinetics have extremely small rate constants, k^0 often less than ~1×10^{-6} cm s^{-1}, which fall outside the quasi-reversible range appropriate for the Nicholson analysis. Instead, for widely separated peaks in CVs sometimes having ΔE_p values larger than ~400 mV, another approach must be employed. Such analysis yields transfer coefficients α, which are obtained via use of the following expressions [3,49].

$$|E_p - E_{\frac{p}{2}}| = 1.857\left[\frac{RT}{\alpha F}\right] = \frac{47.7}{\alpha} \quad (7)$$

where E_p is the peak potential, $E_{p/2}$ is the half-peak potential and

$$E_p = E' + \frac{RT}{\alpha F}\left(0.78 - \ln k^0 - \ln\left(D\alpha nF/RT\right)^{1/2}\right) - \frac{RT}{2\alpha F}\ln v \quad (8)$$

where E' is the formal potential, n is the number of electrons transferred (1 if referring to the hexacyanoferrate II/III system) and v is the scan rate. By estimating α from Equation (7) and then substituting it in Equation (8), along with the known value of D for each anion, enables the determination of values of k^0. One such analysis performed using hexacyanoferrate II/III in 0.5 M H_2SO_4 on various BDD electrodes, including some anodically polarised in acids, produced very low transfer coefficients (α values of only 0.2–0.3) and small HET rate constants k^0 ranging from 2×10^{-5} cm s^{-1} to 40×10^{-5} cm s^{-1} [49].

3. Discussion

Clearly there are a number of factors that can influence the measured ΔE_p values evaluated from cyclic voltammetry, leading to wide variations in HET k^0 values, which in turn can be interpreted as ISET or as OSET processes. It is interesting to note that much of the older literature tends to suggest that the hexacyanoferrate II/III couple is an OSET process, although this view seems to be changing, as more examples of the influence of the electrode surface, indicative of ISET are found. This is especially true for carbon-based electrodes, which may possess a range of different surface functional groups, including carbonyls, carboxylic acids (or carboxylates), anhydride groups, epoxides, and peroxy groups, esters as well as sometimes even phenol and quinone groups, amongst others [17,44,55,91,92] Furthermore, microstructural defects such as missing carbon atoms, dangling bonds, metallic impurities, and folds in thin graphene sheets can also occur, which may affect the HET process. Adsorbed oxygen may also play a role in an ET process occurring on such electrode surfaces as described earlier [93,94].

3.1. The Influence of Functional Groups and Microstructural Features on Carbon Electrodes Electron Transfer Properties

Some functional groups appear to promote electron transfer, which has been reported for example with hexacyanoferrate III reductions conducted on single-walled carbon nanotubes SWCNT [95]. In this case, nanotubes aligned with exposed ends on cysteamine-modified gold electrodes exhibited quite small ΔE_p values of 72–80 mV and relatively fast ET kinetics. Much larger ΔE_p values and thus slower kinetics were measured, however, on randomly dispersed SWCNTs, ranging from an initial value of 204 mV, 2 h after preparation dropping to 94 mV after 6 h and then increasing again to 146 mV after 8 h. The formation of carboxylic acids and quinones at the SWCNT ends, detected by XPS was thought responsible for the increased ET rate in the aligned SWCNT case. This result has, however, been called into question, as the process used to produce the SWCNTs resulted in an increased number of shorter nanotubes, most likely possessing an enhanced number of more active edge plane sites, thereby enhancing the HET kinetics [94].

Carbon-based materials are heterogeneous in nature and can behave in an anisotropic fashion [44]. Their utilisation in electrochemical studies has been explored in numerous

studies. Carbon-based electrodes, whether graphite, graphene, highly oriented pyrolytic graphite (HOPG), Boron Doped Diamond (BDD), or other C-electrode (e.g., carbon paste, carbon fibre, screen printed carbon or pencil graphite), may contain carbon in different forms. Most commonly graphite consists of covalently bound carbon in a planar lamellar sp^2 hybridised hexagonal lattice, which stacks on top of each other due to the weak attractive van der Waals forces to form a three-dimensional lattice comprising basal planes. The ends may contain sp^3 hybridised edge planes. Diamond is another carbon allotrope that comprises sp^3 hybridised carbon. Small rolled-up sheets of graphene can form carbon nanotubes while larger structures include fullerenes. These microstructural and nanostructural features may possess very different ET characteristics. It is generally held that basal planes are far less reactive than edge planes, which occur at the end of a carbon sheet or tube, although it has been demonstrated that this is not always the case. For example, freshly cleaved HOPG surfaces can produce highly reactive basal plane surfaces displaying fast, near-reversible ET kinetics as detected by small ΔE_p values [96]. Over time, however, exposure to atmospheric oxygen can slow the ET reaction, as indicated by the observation of larger ΔE_p values, which ranged from an initial 227 mV on the HOPG electrode to 596 mV after 2 h in a hexacyanoferrate II/III solution in 0.1 M KCl (see also Figure 2). In comparison, edge planes exhibited a narrower set of ΔE_p values between 89 mV and 137 mV, although for a much longer time period (up to 24 h). A more gradual increase in ΔE_p with atmospheric exposure was evident in addition to faster HET kinetics overall. It was also reported that multi-walled carbon nanotubes (MWCNT) deposited on the HOPG electrodes exhibited faster kinetics with a steady ΔE_p figure of 66 mV over the same period of time in a 0.05 M KCl and 0.05 M $NaHSO_4$ supporting electrolyte [55]. Larger ΔE_p values were also noted as consecutive scans were carried out, again indicating that the reaction slowed over time, due to the formation of reaction products which then blocked further ET processes. Fast reversible kinetics were found for the MWCNTs for a range of redox probes including the hexacyanoferrate II/III couple. As both the innate ΔE_p values and the rate of decrease in the measured rate constants were much larger for the hexacyanoferrate II/III couple than found on other known redox couples, believed to be outer sphere in nature (e.g., $[Ru(NH_3)_6]^{2-/3-}$, $[Ir(Cl)_6]^{3-/4-}$), it was suggested that the hexacyanoferrate II/III redox couple, long thought to be an OSET in nature, was, in fact, an ISET process, at least on some carbon-based electrode surfaces [18].

In a recent paper, the upper limit of the standard heterogeneous ET rate (k^0) of the hexacyanoferrate II/III redox mediator on carbon basal planes was estimated to be very slow, of the order of $10^{-9}-10^{-7}$ cm s^{-1} [97]. Under certain conditions, however, basal planes of HOPG may well possess an intrinsic ET activity, resulting in far higher k^0 values, notably in planes containing defects, although edges are generally considered more active [98,99]. Graphite, which consists of multilayered graphene, is considered a non-metal or a "semimetal" possessing a small valence band/conduction band overlap (of the order of 60 meV) with a parabolic-shaped dependence of the density of electronic states (DOS) energy on either side of the Fermi level (E_F). In electrolyte solutions, the DOS is generally low enough for it to exhibit a space charge-dominated capacitance response. Consequently, defects such as dangling bonds, metallic impurities, and surface groups can increase the surface DOS, thereby enhancing the ET process, especially near the DOS minimum at the E_F. In contrast, oxygenated surface groups can contribute to electrostatic (Coulombic) repulsion and cause the opposite effect as discussed above [100].

In practice, the electrochemical response on graphitic surfaces may vary considerably, even for surfaces prepared using the same method. As a result, many researchers have employed HOPG, with some high-quality examples having a typical spacing of $1-10$ µm between single crystal domains which is advantageous for OSET redox systems, which are also dependent on the DOS of the electrode and the electronic coupling between the electrode and redox mediator. These are also insensitive to the presence of specific surface groups, as is the case for ISET systems. An outer-sphere redox mediator, therefore, serves as a direct probe of the surface DOS of graphite, without being sensitive to its surface

chemistry. This has, however, been called into question [48]. It was asserted that since the DOS of the semimetallic graphite is orders of magnitude higher than that of the redox species, any variation in the DOS is likely to be less important. A useful analysis was offered by McCreery and McDermott, who concluded that the three main factors influencing the ET rate are the redox mechanism, surface DOS, and the presence of edge planes [44] Another important factor is the contamination of graphitic surfaces upon exposure to ambient conditions which can rapidly decrease the ET rate by several orders of magnitude [18].

3.2. An Alternative Classification System

According to McCreery redox probes on carbon electrodes can be classified into three categories: (i) insensitive to carbon surface termination effects (e.g., FcMeOH, $[Ru(NH_3)_6]^{3+/2+}$); (ii) surface-sensitive and can interact with specific oxygen functionalities (e.g., $Fe^{3+/2+}$ which can interact with carbonyl, –C=O groups); and (iii) surface sensitive, but do not seem to interact with specific oxygen-containing groups [44]. The hexacyanoferrate II/III anions appear to fit into the third category and generally favour ISET, but the effect of adsorption can vary and can be very unpredictable [10]. Other ISET redox couple probes include dopamine, ascorbic acid, oxygen, and NADH, all of which are known to adsorb directly onto electrode surfaces. In contrast, it is believed that OSET redox couple species, are not surface-sensitive and do not generally adsorb onto electrode surfaces. Examples listed by McCreery and later by Banks et al. include $Ru(NH_3)_6^{2+/3+}$, Ferrocene ($Fc^{0/+}$), $IrCl_6^{2-/3-}$, methyl viologen ($MV^{+/2+}$), methylene blue (MB), chlorpromazine ($CPZ^{0/+}$), and $Co(phen)^{2+/3+}$ [10,44]. Species undergoing OSET processes are unusual and, for example, only two are mentioned in one textbook; $Ru(NH_3)_6^{2+/3+}$ and Fe II/III (in the absence of chloride ions) [6]. It appears many researchers since then may have simply assumed that the hexacyanoferrate II/III redox couple always undergoes an OSET process [7,23,24,55].

3.3. The Effect of Surface Films on Glassy Carbon Elecrtodes

Glassy carbon (GC) electrodes are commonly used in many electrochemical investigations. For example, one report of cyclic voltammetry conducted at 50 mV/s on bare GC electrodes in a solution containing 1 mM $K_3Fe(CN)_6$ and 1 M KCl showed reversible redox peaks [101]. For an oxidised GC electrode, however, (treated at 2.0 V (vs Ag/AgCl) for 600 s), the peak currents were much reduced and a less pronounced diffusional tail was evident in the resultant CV curve. CVs conducted on oxidised GC electrodes displayed a more steady state-like character with a limiting current plateau, thought to arise from the presence of an oxide surface or barrier layer with numerous small "micro holes" or fissures acting to allow only restricted solution access to the electrode surface. The formation of a blue/green colour in the electrolyte possibly indicates the presence of Prussian Blue or a similar compound (e.g., Berlin Green), although the authors ascribed this to a "carbon oxide" film.

Using a GC electrode, Noel and Anantharman carried out a series of cyclic voltammetric studies on the hexacyanoferrate II/III redox system in a variety of deaerated electrolytes including sulphates (H_2SO_4, Na_2SO_4) chlorides (NaCI, KCI) and sodium salts (NaOH, NaH_2PO_4, $Na_2C_2O_4$, and trisodium citrate) [102]. Depending upon the scan rate, they observed ΔE_p values ranging from 85 mV to 180 mV, yielding reasonably close HET k^0 values between 1.6×10^{-3} and 3.1×10^{-3} cm s^{-1} in deaerated 0.1 N Na_2SO_4. (which is equivalent to 0.05 M Na_2SO_4.). In their detailed study, a number of different effects including surface preparation procedure (polishing and cleaning), pH variation, use of heat treatments, and chemical and electrochemical surface treatments (surface activation) were evaluated. Their results indicated that anodic polarisation activated the GC surface yielding reproducible results. Furthermore, rate constants obtained through the use of Nicholson's method differed markedly (in deaerated 0.1 N NaCl) for the oxidation of hexacyanoferrate II (39.1×10^{-3} cm s^{-1}) and the reduction of hexacyanoferrate III (1.3×10^{-3} cm s^{-1}). This was attributed to the presence of different surface states of the glassy carbon at the starting potential of each scan. A GC surface consists of bare carbon as well as oxidised functional

groups (such as carbonyl, carboxylate, and quinone) and reduced functional groups (including –COH, –CH_2OH, hydroquinone), which can influence electrode activity. Anions were also found to have a substantial effect on both the measured rate constants and the limiting currents. In particular chloride ions displayed a special activating effect, which was thought to be due to the occurrence of adsorption and mediated electron transfer processes through bridging ligand interactions, indicative of an ISET process. It was concluded that within certain specified potential limits GC seems to have good activity in deaerated acidic, neutral and alkaline media when used with the hexacyanoferrate II/III redox system.

3.4. Boron-Doped Diamond Electrodes

Another commonly used carbon electrode system is Boron-Doped Diamond (BDD) which contains some sp^3 hybridised carbon. Using a similar strategy, Granger and Swain investigated the hexacyanoferrate II/III kinetics on anodised and hydrogenated BDD [50]. Quasi-reversible kinetics were reported in deoxygenated pH 7.2 buffered 1 M KCl solution. An initial ΔE_p value of 70 mV measured at 50 mV/s increased to 198 mV after oxidation of the BDD was carried out in 1 M H_2SO_4. Following acid washing and hydrogen plasma surface treatment, however, the ΔE_p dropped back to 84 mV suggesting that ET for hexacyanoferrate II/III is sensitive to the presence of surface carbon-oxygen functionalities and probably involves sites associated with the hydrogen-terminated portions of the surface. At pH 7.2 oxygen functional groups are likely to be deprotonated and hence negatively charged, which would be expected to repel the highly charged hexacyanoferrate II/III species, increasing the electron tunnelling distance and thus reducing the rate of electron transfer. Further investigations conducted at low pH (1.8) showed, however, that the inhibition of the HET kinetics was not due exclusively to electrostatic repulsions. The results from the surface treatments conducted in the study also ruled out the influence of adventitious nondiamond carbon phases as the sole sites for electron transfer. It was therefore concluded that diminished hexacyanoferrate II/III kinetics was due to a site-blocking effect arising from the presence of the oxygenated carbon species which could be regenerated following acid washing and plasma hydrogenation treatments, leaving hydrogen-terminated surface moieties.

3.5. Graphene Electrodes

In recent years, 2D graphene has aroused a lot of interest in the electrochemical community. One recent review outlines the use of heteroatom-doped graphene to further improve the performance of this material in a wide range of applications in the energy conversion and storage technologies areas [103] [There are numerous reports in the literature concerning the use of graphene as a highly conductive and even electrocatalytic electrode material, assessed with the aid of the hexacyanoferrate II/III redox probe [63,104–107]. Using potassium hexacyanoferrate III as a redox probe, amongst others, the electrochemical activity of SWCNTs, pristine graphene oxide (GO) nanosheets, chemically and electrochemically reduced GO nanosheets was explored using cyclic voltammetry (conducted at 50 mV/s in 0.1 M KCl) [108]. As expected, a large peak-to-peak separation ΔE_p value of ca. 247 mV was obtained on the GO nanosheets indicative of a slow HET rate, significantly greater than the ΔE_p value of 90 mV obtained on a GC electrode. This was ascribed to the poor conductivity of the GO material and the repulsion of the hexacyanoferrate III by negatively charged surface oxygen species. Both the chemically reduced and electrochemically reduced materials showed remarkably lower ΔE_p values (~90 mV and ~80 mV, respectively), although both were larger than the value found on the SWCNT (ΔE_p of 73 mV). Two reasons were given for this; reduced electrostatic interactions with the hexacyanoferrate II/III species and enhanced conductivity within the reduced GO nanosheets through the reforming of π bonds in the carbon network of the nanosheets.

Fast ET rates were detected in multilayer graphene nanoflake films and in reduced graphene sheet films (rGSF) using the hexacyanoferrate II/III couple [109,110] In the former case, the ΔE_p values varied between 61.5 and 93.2 mV at scan rates varying between

10 mV/s and 400 mV/s, indicative of essentially reversible kinetics. It was stated that these hexacyanoferrate II/III ET reactions proceeded via an ISET pathway and that they appeared to be sensitive to surface chemistry and microstructure, as well as the density of electronic states near the Fermi potential. In the latter case, similar low ΔE_p values ranging between 65 mV and 68 mV in 1 M KCl at 100 mV/s suggestive of fast HET kinetics were found, giving k_{app} values of 4.9 $\times$ 10^{-2} cm s^{-1} for the rGSF and 2.9 $\times$ 10^{-2} cm s^{-1} for a standard GC, respectively.

Studies carried out on Graphene nanoflakes (GNF) of diameter ca. 30 nm were characterised electrochemically after being drop cast onto a boron-doped diamond (BDD) electrode. The flakes were edge-terminated with carboxylic acid (–COOH) or amide functionalities [72] and their reactivity was investigated using hexacyanoferrate II/III amongst other redox probes. A marked difference in response was observed at a BDD electrode modified with COOH-terminated GNF in comparison to an unmodified BDD and an amide-terminated GNF electrode. The BDD electrode displayed reasonably consistent ΔE_p values of about 65 $\pm$ 2 mV in 0.5 mM hexacyanoferrate III in 0. 1 M Phosphate buffer solution (PBS) ranging from pH 4.6 to 9.2, indicative of near reversible ET kinetics. On a COOH-terminated GNF electrode, the ΔE_p values were found to be pH dependent, increasing as the pH decreased from ΔE_p of 109 mV (pH 7) to ΔE_p 250 mV (pH 4.6) with slower kinetics at lower pH attributed to a change in the nature of the redox species, formation of an adsorbed film or an interaction with the electrode surface. Further work conducted in different ionic strength solutions (0.01 M, 0.1 M, and 1 M KCl at pH ~6) revealed that the COOH-terminated GNF behaved differently at the lower KCl concentrations. Unlike the BDD and amide-GNF electrodes, which both showed near reversible kinetics in all solutions, in the COOH-GNF case the ΔE_p value increased considerably displaying a near sigmoidal voltammetric plot as expected from an electrode with pinholes in an insulating surface film or as in an array of microelectrodes, somewhat reminiscent of the result reported by Khoo et al. [101]. The addition of KOH brought the pH up to 8.5 and returned the ensuing voltammogram to a more conventional shape, although the ΔE_p was still large, 231 $\pm$ 21 mV. This indicated that solution acidity and electrolyte concentration were both important factors in determining the behaviour of the hexacyanoferrate II/III couple which was believed to be the inner sphere in nature. Such effects as disruption of ion-pairing with solution cations, a propensity to lose cyano ligands, formation of aggregates, which are possible intermediates to Prussian Blue film formation and acid-base equilibria involving interaction with the COOH-GNF leading to protonation of the nitrogen of the cyanide ligands (to possibly form $[H(Fe(CN)_6)^{3-}]$) were all proffered as explanations for the hexacyanoferrate III behaviour. Moreover, at low electrolyte concentrations, the interaction between the electrode and the hexacyanoferrate III will be more significant, as screening by solution ions in the double layer will be less effective. Further work using spectroelectrochemical methods indicated that the hexacyanoferrate III redox reaction was much less influenced by the presence of GNF in D_2O solvent, thus highlighting the role played by readily available protons from both the COOH-GNF and the electrolyte in destabilising the hexacyanoferrate II/III redox couple [110]. The addition of GNF in the solution led to an additional, very intense cyanide stretch IR band, which was attributed to the formation of a new, non-soluble species. No evidence, however, of a new cyano species in the IR spectrum was found when D_2O was used as the solvent. It was suggested then that the instability of hexacyanoferrate II/III anions may be caused by protonation and subsequent decomposition in the aqueous case. The formation of a precipitate from solutions of $[Fe(CN)_6]^{3-}$ and $[Fe(CN)_6]^{4-}$ in the presence of GNF was concluded from ATR-FTIR spectroscopy, but was found not to occur when D_2O was used as the solvent. In general, GNF had much less influence on the redox reaction in D_2O, highlighting the key role played by readily available protons at the graphene nanoflake edge. This calls into question the notion that both hexacyanoferrate II/III species are stable under a wide range of conditions, as was pointed out by McCreery [44]

More recent work conducted by Banks et al. on graphite and graphene flakes included an investigation utilising the hexacyanoferrate II/III redox probe [16]. Considered an inner sphere probe by the authors and using an EPPG as a comparison (with an ΔE_p of 133 mV), graphitic paste electrodes consisting of different flake sizes (with lateral size from 0.5 µm to 1390 µm) displayed ΔE_p values ranging from 106 mV up to 833 mV and HET k^0 values ranging from 1.93×10^{-3} cm s^{-1} to 6.04×10^{-5} cm s^{-1}. Cyclic voltammograms were recorded in deoxygenated 0.1 M KCl at 100 mV/s. The findings correlated with the number of available edge plane like-sites/defects and the faster kinetics of the smaller lateral flake sizes implicated the role of surface structure in terms of oxygenated species in determining the ET kinetics. Five graphene paste electrodes were also examined and showed a similar trend with ΔE_p decreasing from 300 mV to 98 mV as the lateral flake size decreased from 9.4 µm to 1.3 µm with a concomitant increase in HET k^0 from 4.4×10^{-5} cm s^{-1} to 2.71×10^{-3} cm s^{-1}. This indicated that the basal-to-edge plane ratio played an important role in determining the ET kinetics. It was thought that oxygenated species and ligands on the electrode surface may have influenced the observed electrochemical response, unlike the case for outer-sphere probes, which are dependent only on the electronic density of states. As pointed out by Unwin et al., there "has been debate about the potential limitation and reliability of ferricyanide and ferrocyanide redox mediator as kinetic probes for graphene type materials" [111].

In another paper, the Fermi level on graphene was examined using Raman Spectroscopy in conjunction with cyclic voltammetry to provide information on the presence (or absence) of adsorbed atoms or molecules [64]. Three electroactive redox probes with different electrode interaction mechanisms were employed in this study, including potassium hexacyanoferrate II/III. The adsorption state was probed by analysing the G-peak position in the in situ Raman spectrum conducted during the electrochemical experiments. Evidence for the existence of an adsorption state during redox reactions at graphene for hexacyanoferrate II/III was observed with a clear positive shift in the G-peak position. It was also discovered that the OSET redox species FcMeOH and the ISET hexacyanoferrate II/III interacted differently with the graphene. In the former case, after cycling in FcMeOH there was no difference in the voltammogram. However, in the latter redox species, the G-peak position curve indicated that both hexacyanoferrate II/III anions were adsorbed. Adsorption mostly took place on the less ET reactive basal plane surfaces, while local reactive (edge plane) sites largely determined the electrochemical behaviour. Additional effects of the adsorbed species on the graphene surface were also detected, where a slight change in the electrochemical behaviour was ascribed to changes in graphene charge carrier density and surface passivation.

3.6. Highly Oriented Pyrolytic Graphite Electrodes

A further complication involving the use of hexacyanoferrate II/III as a redox probe, this time on HOPG was described by [18]. The exposure of basal plane and edge plane surfaces to organic solvents (acetonitrile, chloroform, or dimethylformamide) arising from either electrode cleaning or through surface modification during deposition of other materials (e.g., carbon nanotubes), passivated the surface making it surface sensitive. Following such treatment, cyclic voltammetry conducted in 0.1 M solutions of NaCl, KCl, and CsCl yielded a range of diminished HET k^0 values from 4×10^{-6} cm s^{-1} (KCl) up to 8.5×10^{-3} cm s^{-1} (CsCl). These values are indicative of bridging ion complex formation prior to electron transfer at the electrode surface. In comparison, a pristine sample showed fast kinetics with a k^0 of ~0.02 cm s^{-1}. The occurrence of an ISET process influenced by cation size and cation adsorption attributes was implicated in this observation.

In fact, it has long been known that cations present in the supporting electrolyte, generally in concentrations far in excess of the hexacyanoferrate II/III and its attendant counter ion, can affect the reaction rate of an ET process [112–115]. Measured HET rates tend to increase when electrolytes comprising cations descending the group 1 alkali metal series from Li down to Cs are employed [50,102,116,117]. More recent studies have confirmed this

finding. For example, Swain et al. investigated the hexacyanoferrate II/III ET rates on BDD thin film electrodes which were treated to remove any adventitious nondiamond sp^2 carbon surface impurity by a two-step acid-based chemical treatment, followed by a hydrogen microwave plasma treatment [118]. This effectively replaced many terminal surface oxygen species with hydrogen, making the surface more hydrophobic. The results indicated that the apparent rate constant k_{app} increased in order from $Li^+ < Na^+ < K^+ < Cs^+$, although this was less than that obtained for other electrodes such as GC and Au. This trend was attributed to a decrease in the hydration sphere surrounding the cation which occurred as the cation became larger, with the largest k_{app} of 1.35×10^{-2} cm s^{-1} being found for CsCl. This redox system was classified as an ISET as the k_{app} showed high sensitivity to surface chemistry and microstructure, as well as surface condition. In addition, values of k_{app} increased with the concentration of electrolyte ascribed to the diminution of the diffuse layer thickness. Using Tafel plots, transfer coefficients α were evaluated and ranged between 0.52 and 0.55, (similar to those obtained by Bond et al. [87,88]) at temperatures between 25 °C and 65 °C whilst the exchange current densities i^0 increased in the order LiCl < NaCl < KCl. These results seemed to indicate the occurrence of an interfacial/double-layer structure of hydrogen-terminated BDD electrodes that was fundamentally different from that formed on sp^2 carbon electrodes such as graphene. It was speculated that hydrogen-terminated electrodes are more hydrophobic, meaning that the arrangement of the surface water molecules is probably different from that taking place in the more hydrophilic oxygen-terminated sp^2 electrodes. Hydration of hydrophobic surfaces is generally thought to be lower and hydrogen bonding maximised, resulting in a slightly lower potential gradient ϕ_2 at the plane of closest approach (IHP in the EDL), which occurs in the following expression (for an oxidation reaction):

$$k^0{}_{app} = k^0 \, exp[\frac{(\alpha - z)F\varnothing_2}{RT}] \quad (9)$$

where k^0 is the true standard rate constant in the absence of a double layer effect, α is the transfer coefficient, n is the number of electrons transferred (in this case 1) and z is the formal charge on the analyte (3- and 4- for $[Fe(CN)_6]^{3-}$ and $[Fe(CN)_6]^{4-}$, respectively) and the remaining symbols have their usual meanings. Equation (9) is the Frumkin-corrected apparent rate constant which accounts for double-layer concentration effects [3,6,119].

For an sp^3 hybridised diamond carbon, the HET rate could be lower than that of an sp^2 carbon electrode under identical conditions, as the water layer at such sp^3 IHP surfaces is likely to be expanded and thus less dense. It is also probably more ordered in an attempt to maximize hydrogen bonding. If this occurs, for example, at hydrophobic diamond surfaces, then this might cause a slightly lower potential gradient, ϕ_2, at the plane of closest approach than would occur at an sp^2 carbon electrode under the same conditions, thereby altering the heterogeneous ET rate constant k^0.

3.7. Gold Electrodes

Gold electrodes can also sometimes be problematic when used with hexacyanoferrate II/III and there is some evidence that cyano species emanating from hexacyanoferrate II/III can react with gold, effectively corroding the gold, albeit over an extended period of time [120]. Further studies using Electrochemical Impedance Spectroscopy confirmed that the charge transfer resistance R_{CT} changed over time, and it was concluded that the gold electrode reacted with the cyano groups from the hexacyanoferrate II/III redox couple over a period of almost 12 h [121,122]. This is perhaps not surprising given that cyanide is used as a lixiviant in the hydrometallurgical extraction of Au from its ores. Further evidence for this was given by Hua et al. who reported that the $Au(CN)_2{}^-$ anion formed through a competitive reaction with the hexacyanoferrate II/III redox species [123].

3.8. The Role of Spectator Cations

Another recent paper reported the role of alkali metal spectator cations in modifying the rate of heterogeneous ET for the hexacyanoferrate II/III redox pair on Pt and Au operating in aqueous conditions [77]. Approaches used included electrochemical methods, such as cyclic voltammetry with rotating disc electrodes and Tafel plots, which enabled the determination of exchange current densities. In addition, molecular dynamics simulations and in situ surface-enhanced infrared absorption spectroscopy (SEIRAS) were also employed. These authors considered the hexacyanoferrate II/III redox couple to be a simple OSET reaction whereby the kinetics were determined largely by noncovalent electrostatic interactions emanating from the surrounding electrolyte solution. Their analysis utilised the Marcus−Hush (MH) theory in preference to the phenomenological Butler–Volmer approach. The exchange current density i^0 increased in the presence of larger structure-breaking ions in the order of $Li^+ < Na^+ < K^+ < Rb^+ < Cs^+$ which was subsequently correlated with a reduction in the solvent reorganisation energy λ decreasing from 0.59 eV to 0.23 eV in the reverse order; $Li^+ > Na+ > K^+ > Rb^+ > Cs^+$. This would suggest an increase of 44 times for the exchange current density i^0 assuming a low H_{AB} (electronic coupling factor due to electronic mixing) of ~0.025 eV, which is typical for the redox reactions of such transition-metal complexes. The authors claimed this was in reasonable agreement with the experimental exchange current density (i^0) measurements, which gave a 113 times increase in its value. The increased i^0 and reduced reorganisation energy λ found for the hexacyanoferrate II/III redox species was attributed to having an increased number of cations and decreased number of water molecules at the electrified interface. Overall, more cations of lower charge density such as the larger Cs^+ ions were thought to be present in the solvation shell of the bulky $[Fe(CN)_6]^{3-}$ and $[Fe(CN)_6]^{4-}$ anions in comparison to the situation with smaller Li^+ ions, both in the bulk solution and at the electrified interface. The authors concluded that weaker hydrogen bonds ensued with larger cations, consequently lowering the effective interfacial static dielectric constant, which was considered to be a solvent–anion structure breaker. At the other end of the scale, smaller high-charge density cations such as Li^+ form stronger hydrogen bonds, making them solvent-anion structure-maker species. Thus, the association of spectator ions with $[Fe(CN)_6]^{3-}$ and $[Fe(CN)_6]^{4-}$ redox centres are thought to influence the energetics of the hexacyanoferrate II/III activated complexes in the transition state, leading to faster rates for systems with the less hydrated large cations such as Cs^+. By using the Marcus-Hush formalism, the solvent reorganisation energy of heterogeneous electron-transfer reactions decreases as the redox centres move nearer the electrode surface. This is supported by models based on the dielectric continuum theory, predicting a decrease in the electron-transfer reorganisation energy with decreasing distance between the redox centre and the electrode surface further supported by classical molecular dynamics (MD) simulation calculations. Evidence for this claim was based on SEIRAS measurements, which showed an increasing fraction of weakly H-bonded water molecules (in the order of $Li^+ < K^+ < Cs^+$) and a decreasing fraction of strongly H-bonded water molecules (in the order of $Li^+ > K^+ > Cs^+$). Furthermore, it is contended that the cation-dependent properties of the interfacial solvation environment also extend to the static dielectric constant, which is much lower than that of the bulk water (78) and decreases from Li^+ (18) to Cs^+ (3). In addition, this argument is in agreement with the predicted reaction entropy using the Born model and the experimental results meaning that a hydrophobic interface with weakly H-bound water exhibits lower dielectric constants than the hydrophilic surfaces. The authors pointed out that this may have broader implications for the role of structure-making/breaking spectator ions on redox reactions involving hexacyanoferrate II/III species in concentrated electrolytes and ionic liquids.

Dating back to the 1980s, studies have demonstrated that the adsorption of hexacyanoferrate II/III species on metal electrodes is considered an important step in the HET reaction [124]. Ion-pairing with alkali-metal cations may stabilise certain surface-adsorbate orientations, which accounts for the spectra of the adsorbed species observed by Raman and infrared spectroscopies and the behaviour of the spectra with changes in cation and

with electrode potential. Although this simple model did not account for large changes in electronic structure which must occur upon adsorption and which must be important in determining the kinetics of the redox reaction, this led to a qualitative understanding of the nature of such intramolecular interactions. Similar cation-dependent kinetic behaviour was later determined using a RDE assembly on both Au and Pt electrodes [125]. It was suggested that the cation-dependent kinetics of hexacyanoferrate II/III redox species are unlikely to be derived from the positively charged interface, indicative of an ISET process because Pt is likely to have less positive charge than Au near the equilibrium potential of $[Fe(CN)_6]^{3-}$ and $[Fe(CN)_6]^{4-}$, which is around 0.9 V(vs RHE) due to the higher potential of zero charge of 0.72 V (vs RHE) on Pt, than 0.62 V (vs RHE) on Au.

3.9. The Potential of Zero Charge

It is well known that anion participation in the Electrical Double Layer (EDL) structure can also be important [102,126]. This is especially true for oxidation reactions, such as the oxidation of hexacyanoferrate II to hexacyanoferrate III (ferrocyanide to ferricyanide, $[Fe(CN)_6]^{4-}$ to $[Fe(CN)_6]^{3-}$) since they usually occur at potentials more positive than the Potential of Zero Charge (PZC). Anions can be attracted to or repelled from the EDL by the surface charging process, and they may also assume different conformations on the electrode surface [127]. For example, kosmotropic anions (strongly hydrated anions), such as high charge density sulphate, phosphate, and most probably both hexacyanoferrate anions are known to strongly interact with surfaces [41,64], thereby altering the PZC. This PZC shift normally causes an increase in the oxidation potential, thus making the oxidation process less favourable [39,40]. Strong surface interactions such as these may also block some catalytic sites resulting in a diminution of the overall current [127].

Over the years, the hexacyanoferrate II/III redox system has been investigated both below the PZC at negative charge densities, where the double layer effect is pronounced, and above the PZC at positive charge densities, where the electron transfer kinetics are often rapid. Experimental data have shown clearly that the reactant interacts strongly with alkali metal cations forming ion pairs so that the charge on the reacting species transported through the double layer is effectively negative [112,114]. Calculations based on double-layer data for the Hg/0.1 M NaF interface allowed estimates of the apparent transfer coefficient α_a to be made, assuming that the true value of α was independent of electrode potential for this single ET reaction [40]. Starting at negative potentials the value of α_a was found initially to be less than 0.4 and decreased slightly as the electrode potential approached the PZC to a value nearer 0.2. This was interpreted by considering the ET reaction site to be located further away from the electrode surface in the diffuse layer of the EDL. In the vicinity of the PZC, however, the value of α_a increased rapidly, reaching a value close to 1.0 before falling again to about 0.6 as the potential became more positive. This trend was in broad general agreement with experimental data. Complex potential-dependent transfer coefficient behaviour is predicted by Marcus–Hush theory for HET reactions. Based on this work, it was concluded that charge distribution within the reactant and product of a simple one-electron transfer reaction is an important feature of understanding double-layer effects for transition metal complexes. This may also lead to significant variation in the measured apparent transfer coefficient with electrode potential, giving rise to curved Tafel plots, typical of the occurrence of ISET processes.

Hexacyanoferrate II/III anions are quite large bulky inorganic ions with high charge densities. It is estimated that the ferricyanide ion's diameter is about 620 pm, which is larger than many other common anions, such as sulphate (516 pm) and phosphate (476 pm) [40,128]. Quantum chemical calculations indicated that for the ferricyanide anion the negative charge emanates to a large extent from the nitrogen atoms in the cyano ligands, with only a small positive charge attributable to the central iron atom [40]. Calculations were carried out for both anions using a simple geometrical approximation assuming that each cyano ligand was represented as two contiguous hard spheres, one for the carbon and the other for nitrogen, whose radius was assumed to be equal to its covalent value, to 75 pm.

Then, assuming that the complex is in the electrical double layer, the distance of the centre of this atom from the electrode surface was estimated to be 310 pm. The next carbon atom was located 428 pm from the interface with the central Fe ion at 620 pm. The effective charge for both anions was negative, even at positive surface charge densities, but was much larger at negative charge densities than at positive values with the $[Fe(CN)_6]^{4-}$ possessing a larger negative charge density than its $Fe(CN)_6{}^{3-}$ counterpart. The explanation for this was based on the notion that the inner layer was thicker when Na^+ was the counter ion (it is more highly hydrated than other comparable bulkier alkali metal cations further down the series) so that more of the reactant charge was likely to be in this region where the electrostatic potential is high. Moreover, their calculations showed that for $Fe(CN)_6{}^{4-}$ the central Fe ion's effective charge became less positive. Some changes were also identified in the charge on the ligands and in the length of the Fe-C bond, which was 192 pm for the $Fe(CN)_6{}^{3-}$ and 194 pm for the $Fe(CN)_6{}^{4-}$.

3.10. Surface Modulation

Modulation of the electrochemical kinetics of several OSET mediators, including hexacyanoferrate II/III by Au metal electrodes, beneath a continuous double-layer graphene surface was described by Hui et al. [23]. Graphene was deposited by chemical vapor deposition onto the Au surface. Significant enhancements in the rate of electron transfer were determined using a Scanning Electrochemical Microscope (SECM) instrument. On Au, quoting literature values both hexacyanoferrate II and hexacyanoferrate III anions exhibited a standard rate constant k^0 value of 3×10^{-2} cm/s. This was larger than the slower kinetics on graphene which displayed standard rate constant k^0 values of 9.5×10^{-4} cm/s (hexacyanoferrate II) and 1.9×10^{-3} cm/s (hexacyanoferrate III). These values were, however, much less than that reported on the OSET reactant ferrocene, which exhibited fast kinetics with a standard rate constant k^0 value of 1 cm/s on Pt. The results indicated a strong influence of electrode surface; the order of reactivity decreased from Au > graphene/Au > bare graphene. The measured heterogeneous rate constant k^0 values were reported to be 1.4×10^{-2} cm/s, 2.4×10^{-3} cm/s, and 4.0×10^{-4} cm/s, respectively. Thus, the hexacyanoferrate II oxidation reaction determined on graphene/Au was six times faster than on graphene. This enhancement was attributed to the existence of an increased electronic density of states due to an electron-donating effect from the underlying metallic substrate, which also enhanced the electron density of states and the Fermi level of graphene.

Generally, OSET reactions are considered to proceed through direct tunnelling or perhaps hopping of electrons between redox species and the electrode surface. They do not involve an intimate interaction between a reactant or product and an electrode surface nor an adsorbed or catalytic intermediate species [3,4]. Hui et al. noted that according to microscopic theories of electron transfer, such as the Marcus–Hush theory, overlap between the electrode and reactant wave functions, as well as the DOS of the electrode, can influence the electrochemical rate constant leading to differences between electrode materials for the same ET reaction [97]. For example, it is known that CVD-graphene electrodes can exhibit significant kinetic limitations in comparison to their metal counterparts [71,129,130]. In addition, the number of graphene layers [100,131] and the presence of defects [47,111,129–131], can also influence their electronic properties. Alternative explanations including contributions from sub-surface Au through pinholes and doping effects from Au were also considered but were dismissed based on experimental evidence.

3.11. Treated Boron-Doped Diamond

On Boron-Doped Diamond (BDD) electrodes, the removal of carbon-oxygen surface species (such as carboxyl groups) through acid washing and hydrogen plasma treatment was reported to be an effective way to lower ΔE_p and increase the HET rate constant, k^0 [50]. In this case an ISET mechanism was proposed. Anodic polarisation of BDD electrodes substantially increased ΔE_p from initial values of 70 mV (vs SCE) up to 198 mV (vs SCE) in 1 M KCl and 50 mM phosphate buffer pH 7.2, reducing back to 84 mV after the re-

hydrogenation treatment. The anodisation effect was initially ascribed to the electrostatic repulsion of the highly negatively charged hexacyanoferrate II/II species by negatively charged surface oxygen species, thereby increasing the electron tunnelling distance and reducing the electron transfer rate. Another negatively charged redox couple $IrCl_6^{2-/3-}$ which is known to undergo OSET, possesses an E^0 near the valence band of BDD (0.6 V (vs SCE)), however, showed similar behaviour. Its ΔE_p values remained virtually unchanged at both pH 1.8 and pH 7.2 after initial scans, then anodic polarisation, and finally, re-hydrogenation treatments. It was concluded that rather than hexacyanoferrate II/III being influenced by surface charge repulsion from carbon-oxygen groups, the redox couple was subject instead to site-blocking effects through a specific surface interaction with hydrogen-terminated carbons which carbon-oxygen groups prevented, resulting in an ISET process.

3.12. Spectroscopic Studies and Adsorption

As long ago as 1985, Fleischmann et al. demonstrated the adsorption of hexacyanoferrate II/III with Surface Enhanced Raman spectroscopy [124] and SNIFTIRS confirmed that during the cyclic voltammetry cyanide dissociated from hexacyanoferrate II/III during its redox reaction [125,132,133] It has been suggested that irreversible adsorption of a "soluble" form of Prussian Blue (PB), bound to the electrode surface through the nitrogen of the CN group occurred on a platinum electrode in the hexacyanoferrate II/III redox couple in 0.5 M K_2SO_4 at neutral pH [134]. PB formed on the electrode surface only when hexacyanoferrate II (i.e., ferrocyanide but not ferricyanide) was used as the reactant and this was thought to occur initially at low potentials. By increasing the potential during the CV scan, the hexacyanoferrate II in the solution was oxidised, whereas the more stable adsorbed hexacyanoferrate II was not. The hexacyanoferrate III thus generated in solution, close to the electrode surface, then reacted with the adsorbed hexacyanoferrate II to form a thin PB layer. When, however, hexacyanoferrate III was used as the substrate, a stable adsorbed layer was thought improbable as the electrode surface would be expected to catalyse its reduction or perhaps decomposition. The formation of a thin porous film of PB via an adsorbed layer of hexacyanoferrate II enabling electron transport would also explain why the PB layer remained thin.

Another spectroelectrochemical investigation also conducted on Pt, but in 1 M KCl was reported by Pharr and Griffiths [135]. Initially, a soluble polymeric hexacyanoferrate compound was thought to form during a CV scan, but only if wide potential limits were used (−0.33 V(vs SCE) to 0.80 V(vs SCE)). It was also found that ΔE_p increased from an initial value of 145 mV to 270 mV after 6 h, indicative of quasi-reversible (slow) kinetics. They attributed this to the formation of soluble mixed valency ferro/ferricyano compounds such as Prussian Blue (PB) or Berlin Green (BG), which adsorb strongly at positive potentials (0.02 V (vs SCE) to 0.42 V (vs SCE)). Such ferric-ferrocyanide and ferrous-ferricyanide complexes can easily desorb or dissolve into solution as hexacyanoferrate III. Some ferrocyanide and to a lesser extent ferricyanide remained adsorbed however, thereby hindering electron transfer and thus lowering the observed HET rate constant (k^0).

More recently, another spectroelectrochemical investigation conducted on thin (2–10 nm) Pt films formed through sputter coating onto silicon ATR wafers was reported [136]. Using attenuated total reflectance-surface enhanced infrared absorption spectroscopy (ATR-SEIRAS), this work confirmed the production of adsorbed hexacyanoferrate II/III intermediates similar to PB under both anodic and cathodic polarisation conditions in 1 M KCl electrolyte. At large oxidation potentials, evidence was also found for the formation of cyanoplatinate complexes, which were ascribed to electrode degradation processes. The results were interpreted in terms of an ISET process occurring for the hexacyanoferrate II/III redox couple under such conditions.

3.13. Outer Sphere and Ion Pairing

It is perhaps somewhat surprising that many molecules assigned as OSET redox probes including FcA^-, $Fe(CN)_6^{3-}$, $Ru(NH_3)_6^{3+}$, and $Fc(MeOH)_2$ appear to adsorb reversibly on Pt electrode surfaces, the strongest adsorption being reported for the cationic $Ru(NH_3)_6^{2+/3+}$ species [20]. This ruthenium hexaammine compound is often considered the archetypal OSET redox probe and this result provides further evidence for the importance of ion-pairing linking the redox reactant to an electrode surface. It does raise an interesting question, however. For what is widely regarded as the pre-eminent OSET species $Ru(NH_3)_6^{3+}$, how is it that it is adsorbed directly onto a Pt electrode surface when according to the conventional view electron transfer happens when it is instead located at or near the OHP and is separated from the surface by a solvent molecule? For an OSET process, a tunnelling mechanism is usually invoked, but an electron transfer with a molecule in intimate contact with an electrode surface must surely be more rapid. This brings into question the conventional view that in the OSET case, the electroreactant is outside the solvent layer adjacent to the electrode surface [3].

Problems associated with the adsorption of ions from a supporting electrolyte, thereby promoting the ISET route, can be circumvented by employing higher levels of ferro/ferricyanide than normal and dispensing with added (supporting) electrolyte [84]. High charge densities and high ionic strength capabilities make both the hexacyanoferrate II/III anions suitable for this approach. In this study, three macrodisk electrodes (3 mm in diamater) along with 12 μm (platinum and glassy carbon) and 10 μm (gold) microdisk electrodes were employed and cyclic voltammetry was conducted in the absence of oxygen, in order to minimise oxygen interference. The results indicated that higher concentrations of hexacyanoferrate II/III (50 mM to 100 mM) in the absence of added 1 M KCl, yielded near reversible voltammograms. Performed at 20 mV/s, the voltammograms were broadly similar to those obtained using conventional conditions (1 mM to 5 mM concentrations in the presence of 1 M KCl). Further, refinement through the application of a correction for the uncompensated resistance showed very good agreement between simulated and experimentally measured CV curves. A slight difference between the hexacyanoferrate II/III anions was apparent, however, on the GC and Au electrodes. Oxidation of the former species led to voltammetric curves more closely aligned with those using the KCl electrolyte than the latter anions based on the reduction reaction. This was attributed to the migration of the hexacyanoferrate II anion to the electrode, which was less pronounced in the reduction of hexacyanoferrate III conducted at lower potentials. More variation was noticeable with the platinum electrode due to adsorption or surface passivation effects. Slight differences between experimental and simulated results at higher magnitude potentials in 50 mM solutions in the absence of an additional electrolyte were thought to arise from density gradients occurring within the nernst (depletion) layer close to the electrode surface, leading to an additional convective mass transport component, which was not accounted for in the simulations. At faster scan rates above 100 mV/s, this was less of a concern, although uncompensated resistance effects became more prominent as currents became larger. Distorted cyclic voltammetric curves were found when lower $[Fe(CN)_6]^{3-}$ and $[Fe(CN)_6]^{4-}$ concentrations (5 mM and 0.5 mM) were used without added electrolyte. Diminished reduction currents at potentials more negative than the potential of zero charges were also observed and attributed to the electrostatic repulsion of the reactant hexacyanoferrate III anion. Such a situation is less likely to occur in the presence of a compact double layer formed in the presence of a higher electrolyte concentration with other charged species in abundance. Once again, the platinum electrode showed a higher susceptibility to variation than the other electrodes. For the hexacyanoferrate III anion reduction process carried out at low concentrations in an unsupported electrolyte, less change was found, although the currents were reduced on both GC and Au electrodes, possibly due to surface passivation and double-layer effects (Frumkin effect). On Pt, these effects were even more pronounced with its cyclic voltammogram mostly devoid of peaks.

On microelectrodes, good steady-state voltammetry was measured at 50 mM concentrations in the absence of KCl electrolyte but was not apparent at lower concentrations.

In summary, high hexacyanoferrate II/III concentrations (~50 mM) appeared to overcome some of the problems associated with diffuse double-layer effects occurring at low anion concentrations and with macrodisk electrode surface areas. Faster potential sweep rates minimised electrode blockage and passivating phenomena that can plague voltammetric studies at microelectrodes.

3.14. The Effect of Hydrophilicity and Hydrophobicity

The effect of decreased hydrophilicity (or enhanced hydrophobicity) on hexacyanoferrate II/III cyclic voltammograms is evident in Figure 3, where some ΔE_p values increased upon exposure to atmospheric oxygen over extended periods of time [31]. At the same time, an increase in the contact angle of the amorphous carbon-based electrode surface occurred indicative of the existence of a more hydrophobic (less hydrophilic) surface. This shows that although near-reversible voltammograms suggestive of OSET were initially recorded, they gradually became more quasi-reversible over time, especially in the case of HOPG illustrated on the right-hand side of Figure 3C, where ΔE_p progressively increased from 67 mV up to 221 mV during the course of the experiment. This example suggests that freshly prepared, more hydrophilic surfaces such as nitrogen-doped HOPG promote faster HET reactions (OSET), while less hydrophilic (i.e., more hydrophobic) surfaces displayed lower k^0 values, reminiscent of quasi-reversible kinetics. Similar trends were also reported in another study by Duesberg et al. who demonstrated that increased hydrophilicity of a pyrolytic carbon surface through the application of an ammonia plasma treatment, resulted in a significantly enhanced HET k^0 of 4.4×10^{-2} cm s^{-1} [65]. It is interesting to compare this with the treated BDD case presented earlier [50], where hydrogenated (deoxygenated) surfaces enhanced the HET rates.

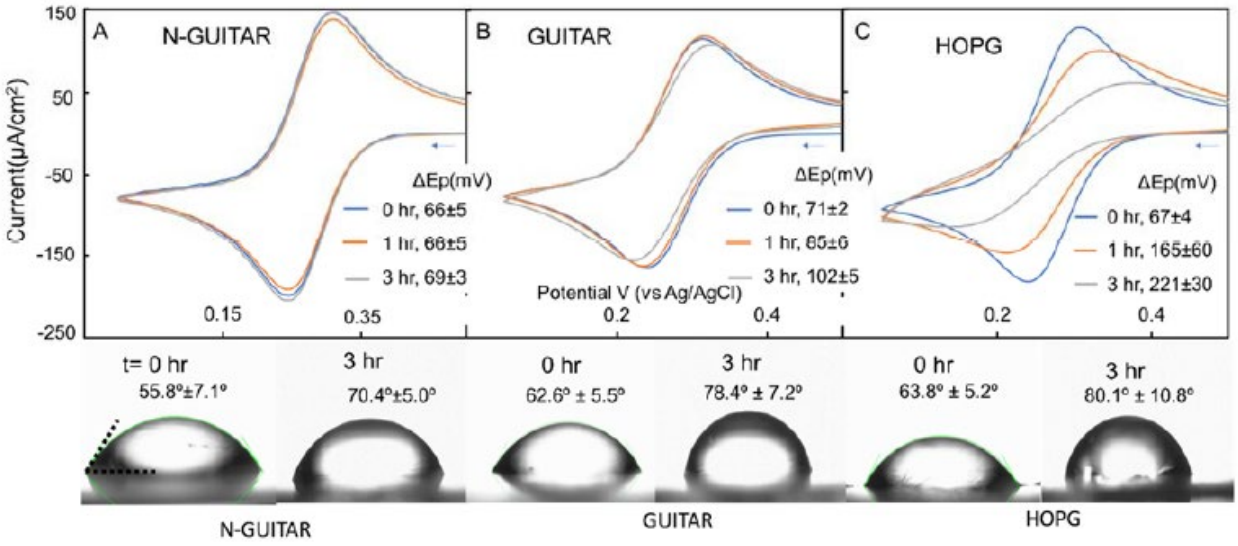

Figure 3. Cyclic voltammograms carried out on various surfaces ranging from a nitrogen-doped amorphous carbon (**A**), to an amorphous carbon (**B**) and a HOPG (**C**) showing changes in peak separations ΔE_p over time. Results were obtained in 1 mM hexacyanoferrate II/III in 0.1 M KCl at a scan rate of 50 mV/s in aerated (oxygenated) solutions [31].

These studies, along with others, strongly suggest that the electrode surface energy and the adjacent water structure in the IHP can affect the EDL and hence alter the HET reaction kinetics. The flux of redox reactants such as hexacyanoferrate III ($[Fe(CN)_6]^{3-}$) or hexacyanoferrate II ($[Fe(CN)_6]^{4-}$) to an electrode surface can also depend upon the thickness of the diffuse double layer and the depletion layer [3,127]. Typically, a diffuse EDL thickness will decrease as the concentration of an electrolyte is increased, causing a

larger potential drop. A higher electric field is therefore experienced by a redox probe as indicated by Equation (5) earlier [137].

3.15. Assessment of Electrochemically Active Surface Area

Given its low cost, ready availability, and well-documented properties (such as well-characterised diffusion coefficient values), it is perhaps not surprising that hexacyanoferrate II/III has been widely used to determine the electroactive surface area EASA, also known as the electrochemically active surface area ECSA, of many electrode surfaces. Assessment of EASA requires the use of a redox couple possessing fast ET kinetics and hence low (near-reversible) ΔE_p values [138]. An example of such a probe is $Ru(NH_3)_6^{2+/3+}$. Unlike the hexacyanoferrate II/III redox couple, this ruthenium-based redox system does not appear to show any changes in its electron transfer rates arising from surface chemistry effects. Consequently, it is entirely dependent upon an electrode's electronic structure (Density of States (DOS)) and the redox probe molecule's Fermi level, enabling accurate estimations of the actual electroactive surface area to be achieved [10]. It is often considered a model OSET redox couple.

Materials investigated using the EASA approach include both metallic and non-metals such as carbon-based materials ranging in size from small nanosized electrocatalysts up to macro-scale electrodes. However, examples abound in the literature of the use of hexacyanoferrate II/III use for this purpose [139–144]. Concerns highlighted in the above discussion serve as a warning regarding the use of this couple in such an application. Ideally in order for either the commonly used Randles–Ševčík cyclic voltammetric approach or the chronoamperometric method utilising the Cottrell equation, a redox probe species should behave in a well-established highly reproducible manner [3,10,138]. Another approach that is sometimes used to elucidate the EASA/ECSA is to utilise the double layer capacitance (C_{dl}) expression using the expression:

$$C_{dl} = \frac{A\varepsilon\varepsilon_0}{d} \tag{10}$$

For example, the EASA of a porous nitrogen-doped carbon electrode was calculated using this double-layer capacitor model in conjunction with hexacyanoferrate II/III where ε is the electrolyte dielectric constant, ε_0 is the dielectric constant of a vacuum, d is the effective thickness of the double layer (charge separation distance) and A is the EASA [144]. Capacitance values can be obtained from cyclic voltammetric or more usually electrochemical impedance spectroscopic investigations, utilising an equivalent circuit model approach to determine C_{dl} values.

In all cases involving the estimation of EASA/ECSA, a redox probe system should undergo entirely diffusion-controlled electron transfer without any surface interactions interfering with the ET process. Unfortunately, this is not always the case with hexacyanoferrate II/III redox couple as highlighted in this report.

3.16. ISET and OSET Terminology

After reviewing the literature, it appears that except in some exceptional circumstances, the hexacyanoferrate II/III redox couple generally falls into the category of an ISET system. However, it does raise the question of whether such terminology (ISET/OSET) is appropriate. While the terminology was first applied to transition metal complexes in solution, it has also been applied to organic compounds [145]. Although this terminology has become more widespread in recent years, many of the issues surrounding its use, such as classification based on experimental validation are seldom addressed. A recent attempt to classify OSET and ISET processes is discussed in a recent textbook, which describes the outer sphere ferrocene probe in aprotic solvents, which is essentially independent of electrode materials, both metallic (Pt and Au) and non-metallic (C) [3]. In this text, a chapter mentions OSET and ISET classification systems based on ionisation potentials (energies) and electron affinities, but the hexacyanoferrate II/III system ($[Fe(CN)_6]^{3-}/[Fe(CN)_6]^{4-}$) is not addressed.

For the hexacyanoferrate II/III to be an OSET process, an adiabatic electron transfer would be favoured with low ΔG values and fast kinetics [3,144]. In contrast, for many ISET processes, including the technologically important hydrogen ion reduction reaction, it is well-known that exchange current densities i^0 may vary enormously (over many orders of magnitude), which is ascribed to the differing electrode surface adsorption energies of hydrogen atom intermediates. A similar situation arises with the oxygen reduction reaction. Both reduction processes are thus labelled as inner sphere (ISET) processes, together with many other technologically important electrochemical reactions involving alcohol oxidation, CO_2 reduction, oxidation of NH_3, hydrogen peroxide oxidation/reduction, electrodeposition, and gas evolution [3].

Perhaps a better description of electron transfer in the hexacyanoferrate II/III system is that essentially it occurs on a surface-sensitive electrode in a quasi-reversible manner in the Inner Helmholtz Plane (IHP) of the EDL. Conversely, the well-known $Ru(NH_3)_6^{2+/3+}$ redox probe is considered to be a surface-insensitive ET system, which generally acts in a reversible (or near reversible) ET manner in the Outer Helmholtz Plane (OHP) of the EDL. This is usually depicted in EDL diagrams in which the OSET case is represented by a transition metal complex oriented such that electron transfer occurs through an intervening solvent molecule on the electrode surface, electron transfer taking place through a tunnelling mechanism [3,4,6]. In the ISET case, however, ET is normally envisaged occurring through a bridging ligand involving a reactant, intermediate, or product that is in direct contact with the electrode surface [3,4,6].

Outer-sphere redox mediators are deemed to be surface insensitive, as the HET rate constant k^0 is not influenced by (i) the presence of surface carbon-oxygen species on carbon electrodes, (ii) the existence of a surface coating of a monolayer film of uncharged adsorbates, or (iii) specific adsorption to surface groups/sites [44]. Thus, in OSET, there is no chemical interaction or catalytic mechanism involving an adsorption process involving the surface or a surface group. These systems often have low reorganisation energies λ, the electrode merely serving as a source or sink of electrons. OSET systems are, therefore, sensitive only to the electronic structure of the electrode material due to its electronic DOS distribution.

For inner sphere redox mediators, such as hexacyanoferrate II/III, which are surface-sensitive, k^0 is strongly influenced by the electrode surface chemistry and microstructure through specific electrocatalytic interactions [44]. These may be inhibited if the surface contains adsorbates or impurities. Such ISET processes can also depend strongly on the presence (or absence) of specific oxygenated species, which may give rise to either beneficial or detrimental effects. They are normally affected by the surface state/structure and/or require a specific surface interaction, being catalysed (or inhibited) by specific interactions with surface functional groups (adsorption sites) rather than the electronic DOS. These ISET systems generally have higher reorganisation energies λ as described in the Marcus-Hush ET formulation.

3.17. Inner and Outer Sphere Reorganisation Energies

There is unfortunately also some confusion in the electrochemical literature caused by the use of the terms *inner sphere* and *outer sphere* when referring to reorganisation energies, λ [3]. Specifically, this addresses the inner sphere and outer sphere components of the reorganisation energy λ, defined in the Marcus–Hush formulation of ET kinetics [3,5–7,144]. The first component, the inner sphere reorganisation energy λ_i involves fluctuations of bond lengths and possibly bond angles and refers to the distortion of the inner coordination shell in the transition state. Any such changes involving the cyano ligands in the hexacyanoferrate II/III transition state are, however, likely to be minimal. The other component, the outer sphere reorganisation energy λ_o, arises from electrical fluctuations of charge distribution, which results in the rearrangement of solvent dipoles between the reactant and the transition state, causing changes within the surrounding solvent sheath. These effects occur during transition state formation, but unlike the ISET and OST reaction processes do not

specifically refer to the reaction location in the vicinity of the electrode surface [3,6,86]. In comparison, for homogeneous electron transfer reactions, the inner sphere reorganisation energy essentially corresponds to the vibrational distortion of the donor–acceptor complex, while the outer sphere component corresponds to solvent rearrangement, which often dominates [146].

It has been pointed out [3] that even if there is not a strong interaction with an electrode (i.e., an OSET process takes place) the kinetics of the ET reaction can still be dependent on the electrode material for a number of reasons; including (a) double-layer effects (b) the effect of the metal on the structure on the IHP (hydrophobicity) and (c) the effect of the energy and distribution of electronic states (DOS) in the electrode.

Recently, Seri [147] determined the HET k^0 to be 5.0×10^{-2} cm s^{-1} in a hexacyanoferrate II to III oxidation study utilising a Pt electrode in deaerated 1 M KCl. Using a differential form of the Tafel equation, the anodic transfer α_a was estimated to be 0.51, very close to 0.5. In another recent study, employing a similar procedure, Roth et al. conducted a careful investigation of the reduction of ferricyanide on Au [148]. A cathodic transfer coefficient α_c of 0.40 was obtained in this study and a lower HET k^0 figure, estimated to be 5.9×10^{-3} cm s^{-1} was measured in 0.1 M KCl. This was derived from the expression relating the exchange current density i^0 to the HET rate constant k^0 (Equation (11)), although this figure is based on the Au electrodes's geometric area and is likely to be an upper limit, as the EASA/ESCA is in fact probably larger, thereby reducing both i^0 and k^0

$$i^0 = Fk^0\left(C_{ox}^{(1-\alpha)}C_{red}^{\alpha}\right) \tag{11}$$

Both of these kinetic studies were conducted on metallic electrodes (Pt and Au), yielding transfer coefficients (α) close to 0.5, as expected for a simple one electron transfer process.

In contrast, Fletcher suggested the occurrence of an E$\hat{C}$ mechanism on carbon fibre random array microelectrodes (RAM) for the reduction of hexacyanoferrate III [149]. A cathodic (reduction) transfer coefficient α_c of 1 was ascertained from a Tafel slope, b_c of 61.7 mV/decade, emanating from a CV carried out at 20 mV/s in deaerated 0.5 M KNO_3. The Tafel plot was linear over two orders of magnitude, demonstrating no dependence of the transfer coefficient α_c on potential, as predicted from the Marcus–Hush formulation of ET processes in the situation where the reorganisation energy λ is significant (possibly above ~100 kJ mol^{-1} or ~1 eV). In this case, if the Tafel slope was indeed curved, then the potential dependence of the transfer coefficient would arise from the following relationship:

$$\alpha = \frac{1}{2} + \frac{F\left(E - E^{0'}\right)}{4\lambda} + \frac{\Delta w}{2\lambda} \tag{12}$$

where the term Δw is the work term difference between reactants and products, as a result of changes in free energies associated with the respective equilibrium constants [145]. To account for this linear Tafel plot, a two-step E$\hat{C}$ mechanism was suggested to take place on the carbon microelectrodes. It is possible that this may involve adsorption of the hexacyanoferrate III or even carbon surface-based ion-pairing involving K^+ in the second rate-determining step [150] as indicated in the following scheme: [102].

$$K^+ + Fe(CN)_6{}^{3-} \rightleftharpoons [K.Fe(CN)_6]^{2-} \text{ (C)} \tag{13}$$

$$[K.Fe(CN)_6]^{2-} + e^- \rightleftharpoons [K.Fe(CN)_6]^{3-} \text{ E} \tag{14}$$

$$[K.Fe(CN)_6]^{3-} \rightarrow [Fe(CN)_6{}^{4-}]_{aq} + K^+ \hat{C} \tag{15}$$

where the number of electrons involved in the electrochemical step E is 1 (i.e., $n_p = 1$), the number in the rate determining step $\hat{C}$ is 0 ($n_q = 0$) and the number of electrons involved in any following steps is also 0 ($n_r = 0$). This leads to the following description of the transfer coefficient for the cathodic reduction given by Equation (16)

$$\alpha_c = n_p + n_q\beta = 1 \tag{16}$$

where β is the symmetry factor (normally 0.5), which in turn is represented by the expression (for a reduction reaction) in the Marcus–Hush ET treatment as:

$$\beta = \frac{1}{2}\left[1 - \frac{F\eta}{2\lambda_m}\right] \quad (17)$$

Then, the resultant Tafel slope b_c is given by

$$b_c = \frac{\partial\eta}{\partial \log i} = \frac{2.303RT}{\propto_c F} = 59.2 \text{ mV/decade} \quad (18)$$

Here, the overpotential η, is defined as the difference between the applied potential E and the equilibrium potential $E_{eq.}$This result is consistent with the notion that a one-electron transfer electrochemical step occurs (labelled E), which is then followed by a rate-determining chemical step (denoted by Ĉ). For many organic reactants, the latter process is often a rearrangement (or in the case of hexacyanoferrate II/III, possibly a carbon electrode surface process involving ion-pairing [102]). Comparable Tafel slopes were also measured for other OSET redox species; potassium hexachloroiridate III (b_c of 59.9 mV/decade) and ferrocene in butyltrimethylammonium bis(trifluoromethylsulfonyl) imide (b_c value of 63.5 mV/decade), indicating that all shared a similar EĈ mechanism on the RAM electrodes. Furthermore, in contrast to the older Frumkin work, which showed a curved Tafel plot on Hg [80] these Tafel plots were all remarkably linear, displaying linearity over at least two orders of current magnitude.

3.18. Future Perspectives

Finally, it should be noted that the future exploration of hexacyanoferrate behaviour in non-aqueous or even mixed electrolytes could well provide a useful way to discriminate between the ISET and OSET processes. Solvents such as (room temperature) ionic liquids ((RT)ILs), deep eutectic solvents (DES), and even possibly mixtures of the two, could provide useful information as their higher viscosities and lower hexacyanoferrate II/III species ($[Fe(CN)_6]^{4-}$ and $[Fe(CN)_6]^{3-}$) diffusion coefficients may well provide valuable insights into their ET mechanisms. In one study, HET rate constants for hexacyanoferrate II/III in the DES Ethaline on a GC electrode was reported, and a comparison was made with several RTILs, in addition to conventional aqueous and acetonitrile solvents [151]. In this work, special attention was given to accounting for ohmic drop effects in the higher-viscosity solvents. The rate constants measured in the DES ethaline were about half that measured in conventional solvents. For the RTILs investigated in this work, the rate constants were even lower (typically by around two orders of magnitude). The results were interpreted in terms of the solvent relaxation time described in the Marcus–Hush ET theory for an adiabatic electron transfer process. In this case, where the inner sphere structures of the hexacyanoferrate II/III are very similar, the solvent reorganisation in the outer sphere component dominated the activation energy of the ET process.

The hexacyanoferrate II/III redox couple was also examined on Au, Pt, and GC electrodes in twelve ILs and in three chloride-containing DES (ethaline, propaline, and glyceline) [152]. In the latter solvents, peak separations were between 70 and 90 mV, giving HET rate constants ranging from 1.39 to 7.6 × 10^{-4} cm s^{-1} compared to a far higher (order of magnitude) value of 1.3 × 10^{-3} cm s^{-1} in an aqueous solution. The DES exhibited a rate constant almost 10 times higher than in the IL 1-*n*-butyl-1-methylpyrrolodinium bis(trifluoromethylsulfonyl)imide. In some less viscous ILs ΔE_p, values of 70–80 mV were measured at slow scan rates (<20 mV/s) with rate constants of approximately 10^{-4} cm s^{-1} whereas Ils with viscosities greater than 0.5 Pas displayed rate constants an order of magnitude lower. As in many aqueous electrolytes, adsorption was found to ensue on some electrodes, notably Au, and in some instances on Pt and GC as well. It was also reported that under atmospheric conditions slow oxidation or reduction processes took place over periods of time longer than a few hours. Provided, however, a freshly prepared hexacyanoferrate II/III solution was used within this time period, it was generally thought

stable enough to be used as a redox probe, although solubility issues were apparent in some hydrophobic RTILs. The authors concluded that with a few exceptions, the hexacyanoferrate II/III was stable enough to be employed as a redox probe in such solvents. By varying the ions present in these solvents and other conditions, (such as electrode material) these results suggest that they would serve as useful media for the exploration of ISET or OSET processes involved in the hexacyanoferrate II/III redox system.

In another recent report, the hexacyanoferrate II/III couple serving as a model redox probe was examined in a range of potassium fluoride concentrations up to 17 M [153]. Such highly concentrated "water-in-salt" electrolytes are of potential interest in future energy storage devices. On freshly cleaved HOPG electrodes a number of observations were made. Firstly the PZC dropped from 0.1 V(vs Ag/AgCl) at 1 M KF to −0.4 V (vs Ag/AgCl) at 17 M KF. An increased level of hydrophobicity was also determined at higher KF concentrations, with contact angles ranging from 63.8° at 0.5 M KF to 94.4° at 17 M KF). In the presence of 10 mM $K_3Fe(CN)_6$ at 0.5 M KF, large ΔE_p values ranging from 220 mV to 292.5 mV were measured over scan rates from 10 mV/s to 1 V/s, indicative of quasi-reversible kinetics. When higher KF concentrations were used ΔE_p dropped to 116.4 mV for 1 M KF and down to 100.6 mV for 5 M KF at a scan rate of 10 mV/s. The peak separation then dropped even further to 81 mV at 10 M KF (the water-in-salt regime). In addition, the equilibrium and formal potentials changed, moving in a positive manner as the KF concentration was raised. Another notable effect was the lowering of the diffusion coefficients to 1.94×10^{-7} cm^2 s^{-1} at 10 M KF to 1.24×10^{-7} cm^2 s^{-1} at 17 M KF which are similar values to those of RTILs. Under such conditions, the Nicholson analysis described above is no longer applicable, although at lower concentrations in 0.5 M KF, the HET k^0 was ~2×10^{-4} cm s^{-1} and at 5 M KF k^0 was ~4×10^{-3} cm s^{-1} indicative of the ET being more reversible at higher concentrations. A bridge mechanism was suggested to account for this as promulgated by Peter et al. [154]. In this case, the reduced hexacyanoferrate II anion forms part of an ion pair with the alkali metal cation (K^+), and ET occurs through binding with another cation, which is more readily available at such KF concentrations. Furthermore, at the highest levels of KF, the HET k^0 was ~1×10^{-3} cm s^{-1}, possibly due to an additional anion (fluoride) binding effect.

4. Conclusions and Recommendations

This review indicates that there has been considerable ambiguity about the potential limitations and reliability of hexacyanoferrate II/III redox mediators as kinetic probes, especially for carbon electrode materials such as graphite and graphene. Therefore, there now exists a number of reasons for discontinuing the inner/outer sphere (ISET/OSET) terminology for heterogeneous electron transfer when referring to the hexacyanoferrate II/III redox couple as follows:

(a) The ISET/OSET terminology originally referred to specific ligand exchange reactions for octahedral transition metal complexes systems in homogeneous solution-based reactions. In this situation, the solvent can play a significant role through the solvent reorganisation energy term, λ in the Marcus–Hush ET treatment. The use of the terms inner sphere and outer sphere when referring to this reorganisation energy only adds to the confusion. In the original inorganic chemistry literature, there is no mention of adsorption or reference to an electrode surface chemistry, i.e., HET kinetics, although Marcus and Hush later extended it to include an electrode surface as a reactant. At present, in the electrochemical literature, its use has even been extended to organic compounds.

(b) The terminology is redundant, as the terms "surface-sensitive" and "surface-insensitive" can adequately differentiate between simple ET processes and ET processes that are coupled with chemical kinetic reactions, typically displaying slow electron transfer and possibly involving adsorption processes. This gives a better description of the location of the electron transfer reactions and the role of the electrode surface in the ET process.

(c) As a result, it is suggested that serious consideration be given to the use of the term "surface-sensitive" when considering the hexacyanoferrate II/III species in order to better describe inner sphere behaviour. The hexacyanoferrate II/III anion is one such example of this type of surface-sensitive redox system, whereas the $Ru(NH_3)^{2+/3+}$ cation species can be considered as an example of a surface-insensitive redox couple probe.

(d) Although hexacyanoferrate II/III is useful as a redox couple or probe, the experimenter must appreciate the influence of such surface interactions, double-layer structural alterations due to the presence of cations and/or anions and other effects (e.g., solvent effects influencing the outer sphere reorganisation energy and other Marcus–Hush parameters).

(e) Considerable care needs to be taken when assessing EASA (ECSA) using the hexacyanoferrate II/III redox probe molecules and it is probably, therefore, better to use other redox couples such as $Ru(NH_3)_6{}^{3+}$ or $Fc^{0/+}$ depending upon the solvent and probe solubility.

(f) Added redundant terminology introduces confusion, particularly to novice electrochemists. Although hexacyanoferrate II/III is, under certain conditions most probably an outer sphere anion (OSET) reactant, more often it behaves as an inner sphere anion (ISET) reactant, especially in the case of carbon-based electrode materials.

(g) Consequently, consideration should also be given to the use of the term multi-sphere electron transfer (MSET) redox probe, specifically for the hexacyanoferrate II/III redox couple. This may denote either OSET or ISET characteristics, depending upon both electrode structure and surface/interfacial chemistry proceeding at the electrode/electrolyte boundary.

(h) There is a need for an unequivocal method for the classification of redox probes such as the hexacyanoferrate II/III system. At present, this does not appear to be the case and there is a distinct lack of a clearly defined categorisation methodology for redox couples. Although fast ET processes are generally thought to undergo OSET, while slow ones typically suggest ISET, this is not always the case especially where adsorption or intermediate species are involved.

(i) For this reason, it is recommended that more than one type of redox probe be employed. When carrying out electrochemical studies, especially those involving carbon electrode surfaces. In aqueous electrolytes hexacyanoferrate II/III and $Ru(NH_3)_6Cl_3$ are quite often used in order to distinguish between different ET processes usually representing ISET and OSET processes, respectively, on carbon-based electrode surfaces.

In conclusion, there is a strong argument to be made to dispense with the inner/outer sphere (ISET/OSET) terminology in electrochemistry, certainly as applied to the hexacyanoferrate II/III redox couple. Its continued use may give rise to confusion and is often a poor description of the nature of many surface electron transfer processes. In practice, a wide variety of factors can influence the ET process, which is dependent on supporting electrolyte cations, the presence (or absence) of surface oxides and adsorbates, electrode surface energy effects (hydrophobic/hydrophilic effecting the solvent/surface interactions), double layer potential effects (Frumkin correction) and solvent reorganisation effects. In the case of the ISET process, this may well lead to curved Tafel slopes, with potential-dependent transfer coefficient influencing the observed logarithm current/potential behaviour. Thus, it is clear that the observation of differing responses when using varied inner- and outer-sphere redox probes allows insight to be deduced regarding the state of the surface structure of the electrode material in question.

Author Contributions: Conceptualization J.F.C. and A.J.B.; writing—original draft preparation J.F.C. and A.J.B.; investigation R.C.d.C.; writing—review and editing—J.F.C., R.C.d.C. and A.J.B.; supervision J.F.C. and A.J.B.; project administration J.F.C. All authors have read and agreed to the published version of the manuscript.

Funding: This research received no external funding.

Institutional Review Board Statement: Not applicable.

Informed Consent Statement: Not applicable.

Acknowledgments: The authors gratefully acknowledge the award of a DIT (now TU Dublin) *Fiosraigh* Dean of Graduate Studies award to R C de Carvalho, the ESHI and FOCAS Institutes and COST Action MP1407 (e-MINDS).

Conflicts of Interest: The authors declare no conflict of interest.

References

1. Cotton, F.A.; Wilkinson, G. *Advanced Inorganic Chemistry, A Comprehensive Text*, 5th ed.; Wiley-Interscience Publishers: Hoboken, NJ, USA, 1988; p. 1306.
2. Lappin, G. *Redox Mechanisms in Inorganic Chemistry*; Ellis Horwood: New York, NY, USA, 1994; Chapters 1–3.
3. Bard, A.J.; Faulkner, L.R.; White, H.S. *Electrochemical Methods, Fundamentals and Applications*, 3rd ed.; Wiley: New York, NY, USA, 2022; Chapters 3,7,15,17.
4. Zanello, P. *Inorganic Chemistry, Theory, Practice and Application*; RSC: Cambridge, UK, 2003; pp. 7–12+62.
5. Compton, R.G.; Banks, C.E. *Understanding Voltammetry*; World Scientific Publications: Singapore, 2007; pp. 66–76.
6. Schmickler, W.; Santos, E. *Interfacial Electrochemistry*, 2nd ed.; Springer: Berlin/Heidelberg, Germany, 2010; Chapter 9.
7. Gileadi, E. *Physical Electrochemistry; Fundamentals, Techniques and Applications*, 2nd ed.; Wiley: New York, NY, USA, 2018; pp. 68–72.
8. Weaver, M.J.; Anson, F.C. Simple criteria for distinguishing between inner and outer sphere electrode reaction mechanisms. *J. Am. Chem. Soc.* **1975**, *97*, 4403–4405. [CrossRef]
9. Weaver, M.J.; Anson, F.C. Distinguishing between Inner- and Outer-Sphere Electrode Reactions. Reactivity Patterns for Some Chromium(III)-Chromium(II) Electron-Transfer Reactions at Mercury Electrodes. *Inorg. Chem.* **1976**, *15*, 1871–1881. [CrossRef]
10. García-Miranda Ferrari, A.; Foster, C.W.; Kelly, P.J.; Brownson, D.A.C.; Banks, C.E. Determination of the Electrochemical Area of Screen-Printed Electrochemical Sensing Platforms. *Biosens* **2018**, *8*, 53. [CrossRef] [PubMed]
11. Fotouhi, L.; Fatollahzadeh, M.; Heravi, M.M. Electrochemical Behavior and Voltammetric Determination of Sulfaguanidine at a Glassy Carbon Electrode Modified With a Multi-Walled Carbon Nanotube. *Int. J. Electrochem. Sci.* **2012**, *7*, 3919–3928. [CrossRef]
12. Zhu, P.; Zhao, Y. Cyclic voltammetry measurements of electroactive surface area of porous nickel: Peak current and peak charge methods and diffusion layer effect. *Mats. Chem. Phys.* **2019**, *233*, 60–67. [CrossRef]
13. Ngamchuea, K.; Eloul, S.; Tschulik, K.; Compton, R.G. Planar diffusion to macro disc electrodes—What electrode size is required for the Cottrell and Randles-Sevcik equations to apply quantitatively? *J. Solid State Electrochem.* **2014**, *18*, 3251–3257. [CrossRef]
14. McCreery, R.L. Advanced carbon electrodes materials for molecular electrochemistry. *Chem. Rev.* **2008**, *108*, 2646–2687. [CrossRef]
15. Huang, L.; Cao, Y.; Diao, D. Nanosized graphene sheets induced high electrochemical activity in pure carbon film. *Electrochim. Acta* **2018**, *262*, 173–181. [CrossRef]
16. Slate, A.J.; Brownson, D.A.C.; Abo Dena, A.S.; Smith, G.C.; Whitehead, K.A.; Banks, C.E. Exploring the electrochemical performance of graphite and graphene paste electrodes composed of varying lateral flake sizes. *Phys. Chem. Chem. Phys.* **2018**, *20*, 20010. [CrossRef]
17. Ambolikar, A.S.; Guin, S.K.; Neogy, S. An insight into the outer- and inner-sphere electrochemistry of oxygenated single-walled carbon nanohorns (o-SWCNHs). *New J. Chem.* **2019**, *43*, 18210. [CrossRef]
18. Xiong, L.; Batchelor-McAuley, C.; Ward, K.R.; Downing, C.; Hartshorne, R.S.; Lawrence, N.S.; Compton, R.G. Voltammetry at graphite electrodes: The oxidation of hexacyanoferrate (II) (ferrocyanide) does not exhibit pure outer-sphere electron transfer kinetics and is sensitive to pre-exposure of the electrode to organic solvents. *J. Electroanal. Chem.* **2011**, *661*, 144–149. [CrossRef]
19. Griffiths, K.; Dale, C.; Hedley, J.; Kowal, M.D.; Kaner, R.B.; Keegan, N. Laser-scribed graphene presents an opportunity to print a new generation of disposable electrochemical sensors. *Nanoscale* **2014**, *6*, 13613. [CrossRef] [PubMed]
20. Mampallil, D.; Mathwig, K.; Kang, S.; Lemay, S.G. Reversible Adsorption of Outer-Sphere Redox Molecules at Pt Electrodes. *J. Phys. Chem. Lett* **2014**, *5*, 636–640. [CrossRef]
21. Kitamura, F.; Nanbu, N.; Ohsaka, T.; Tokuda, K. A kinetic and in situ infrared spectroscopic study of the $[Fe(CN)_6]^{3-}$/$[Fe(CN)_6]^{4-}$ couple on platinum single crystal electrodes. *J. Electroanal. Chem.* **1998**, *456*, 113–120. [CrossRef]
22. Chen, J.; Aoki, K. Overestimation of heterogeneous rate constants of hexacyanoferrate at nanometer-sized ultramicroelectrodes. *Electrochem. Comm.* **2002**, *4*, 24–29. [CrossRef]
23. Hui, J.; Zhou, X.; Bhargava, R.; Chinderle, A.; Zhang, J.; Rodríguez-López, J. Kinetic Modulation of Outer-Sphere Electron Transfer Reactions on Graphene Electrode with a Sub-surface Metal Substrate. *Electrochim. Acta* **2016**, *211*, 1016–1023. [CrossRef]
24. Duo, I.; Fujishima, A.; Comninellis, C. Electron transfer kinetics on composite diamond (sp^3)–graphite (sp^2) electrodes. *Electrochem. Comm.* **2003**, *5*, 695–700. [CrossRef]
25. Torres, L.M.; Gil, A.F.; Galicia, L.; Gonzalez, I. Understanding the Difference between Inner sphere and Outer sphere Mechanisms. *J. Chem. Ed.* **1996**, *73*, 808–810. [CrossRef]
26. Tanimoto, S.; Ichimura, A. Discrimination of Inner- and Outer-Sphere Electrode Reactions by Cyclic Voltammetry Experiments. *J. Chem. Ed.* **2013**, *90*, 778–781. [CrossRef]
27. De Carvalho, R.C. Synthesis and Novel Applications of Cerium Dioxide. Ph.D. Thesis, Technological University Dublin, Dublin Ireland, 2019.

28. Fanjul-Bolado, P.; Hernández-Santos, D.; José Lamas-Ardisana, P.; Martín-Pernía, A.; Agustín Costa-García, A. Electrochemical characterization of screen-printed and conventional carbon paste electrodes. *Electrochim. Acta* **2008**, *53*, 3635–3642. [CrossRef]
29. Morrin, A.; Killard, A.; Smyth, M.R. Electrochemical characterisation of commercial and home made screen printed carbon electrodes. *Anal. Lett.* **2003**, *36*, 2021–2039. [CrossRef]
30. Kadara, R.O.; Jenkinson, N.; Banks, C.E. Characterisation of commercially available electrochemical sensing platforms. *Sens. Actuators B Chem.* **2009**, *138*, 556–562. [CrossRef]
31. Hamal, K.; May, J.; Zhu, H.; Dalbec, F.; Echeverria, E.; McIlroy, D.; Aston, E.; Cheng, I.F. Electrochemical Aspects of a Nitrogen-Doped Pseudo-Graphitic Carbon Material: Resistance to Electrode Fouling by Air-Aging and Dopamine Electro-Oxidation. *J. Carbon Res.* **2020**, *6*, 68. [CrossRef]
32. Bard, A.J.; Parsons, R.; Jordan, J. (Eds.) *Standard Potentials in Aqueous Solutions*; IUPAC Marcel Dekker: New York, NY, USA, 1985; p. 408.
33. Lide, D. (Ed.) *CRC Handbook of Chemistry and Physics*, 88th ed.; CRC Press: Boca Raton, NJ, USA, 2007–2008; pp. 11–12.
34. Alexander, J.J.; Gray, H.B. Electronic Structures of Hexacyanometalate Complexes. *J. Am. Chem. Soc.* **1968**, *90*, 4260–4271. [CrossRef]
35. Engel, N.; Bokarev, S.I.; Suljoti, E.; Garcia-Diez, R.; Lange, K.M.; Atak, K.; Golnak, R.; Kothe, A.; Dantz, M.; Kühn, O.; et al. Chemical Bonding in Aqueous Ferrocyanide: Experimental and Theoretical X-ray Spectroscopic Study. *J. Phys. Chem. B* **2014**, *118*, 1555–1563. [CrossRef] [PubMed]
36. Kunnus, K.; Zhang, W.; Delcey, M.G.; Pinjari, R.V.; Miedema, P.S.; Schreck, S.; Quevedo, W.; Schroder, H.; Fohlisch, A.; Gaffney, K.J.; et al. Viewing the Valence Electronic Structure of Ferric and Ferrous Hexacyanide in Solution from the Fe and Cyanide Perspectives. *J. Phys. Chem. B* **2016**, *120*, 7182–7194. [CrossRef]
37. Compton, R.G.; Batchelor-McCauley, C.; Dickinson, E.J.F. *Understanding Voltammetry: Problems and Solutions*; Imperial College Press: London, UK, 2012; p. 157.
38. McKay, K.M.; McKay, R.A.; Henderson, W. *Introduction to Modern Inorganic Chemistry*, 6th ed.; Nelson Thornes: Cheltenham, UK, 2002; p. 280.
39. Guo, M.; Kallman, E.; Sørensen, L.K.; Delcey, M.G.; Pinjari, R.V.; Lundberg, M. Molecular orbital simulations of metal 1s2p resonant inelastic X-ray scattering. *J. Phys. Chem. A* **2016**, *120*, 5848–5855. [CrossRef]
40. Fawcett, W.R.; Hromadova, M.; Tsirlina, G.A.; Nazmutdinov, R.R. The role of charge distribution in the reactant and product in double layer effects for simple heterogeneous redox reactions. *J. Electroanal. Chem.* **2001**, *498*, 93–104. [CrossRef]
41. Prampolini, G.; Yu, P.; Pizzanelli, S.; Yang, F.; Zhao, J.; Wang, J. Structure and dynamics of ferrocyanide and ferricyanide anions in water and heavy water: An insight by MD simulations and 2D ir spectroscopy. *J. Phys. Chem. B* **2014**, *118*, 14899–14912. [CrossRef]
42. Moldenhaeur, J.; Meier, M.; Paul, D.W. Rapid and direct detection of diffusion coefficients using microelectrode arrays. *J. Electrochem. Soc.* **2016**, *163*, H672–H678. [CrossRef]
43. Lundgren, C.A.; Murray, R.W. Observations on the Composition of Prussian Blue Films and Their Electrochemistry. *Inorg. Chem.* **1988**, *27*, 933–939. [CrossRef]
44. McCreery, R.L.; McDermott, M.T. Comment on electrochemical kinetics at ordered graphite electrodes. *Anal. Chem.* **2012**, *84*, 2602–2605. [CrossRef] [PubMed]
45. Schwarzová-Pecková, K.; Vosáhlová, J.; Barek, J.; Šloufová, I.; Pavlova, E.; Petrák, V.; Zavázalová, J. Influence of boron content on the morphological, spectral, and electroanalytical characteristics of anodically oxidized boron-doped diamond electrodes. *Electrochim. Acta* **2017**, *243*, 170–182. [CrossRef]
46. Fang, C.S.; Oh, K.H.; Oh, A.; Lee, K.; Park, S.; Kim, S.; Park, J.K.; Yang, H. An ultrasensitive and incubation-free electrochemical immunosensor using a gold-nanocatalyst label mediating outer-sphere-reaction-philic and inner-sphere-reaction-philic species. *Chem. Comm.* **2016**, *52*, 5884–5887. [CrossRef]
47. Gutiérrez-Portocarrero, S.; Roquero, P.; Becerril-González, M.; Zúñiga-Franco, D. Study of structural defects on reduced graphite oxide generated by different reductants. *Diam. Relat. Mater.* **2019**, *92*, 219–227. [CrossRef]
48. Zhang, G.; Cuharuc, A.S.; Guell, A.G.; Unwin, P.R. Electrochemistry at highly oriented pyrolytic graphite (HOPG): Lower limit for the kinetics of outer-sphere redox processes and general implications for electron transfer models. *Phys. Chem. Chem. Phys.* **2015**, *17*, 11827. [CrossRef]
49. Duo, I.; Levy-Clement, C.; Fujishima, A.; Comninellis, C. Electron transfer kinetics on boron-doped diamond Part I: Influence of anodic treatment. *J. Appd. Electrochem.* **2004**, *34*, 935–943. [CrossRef]
50. Granger, M.C.; Swain, G.M. The Influence of Surface Interactions on the Reversibility of Ferri/Ferrocyanide at Boron-Doped Diamond Thin-Film Electrodes. *J. Electrochem. Soc.* **1999**, *146*, 4551–4558. [CrossRef]
51. Niu, P.; Asturias-Arribas, L.; Jordà, X.; Goñi, A.R.; Roig, A.; Gich, M.; Fernández-Sánchez, C. Carbon–Silica Composites to Produce Highly Robust Thin-Film Electrochemical Microdevices. *Adv. Mater. Technol.* **2017**, *2*, 1700163–1700174. [CrossRef]
52. Campanhã Vicentini, F.; Ravanini, A.E.; Figueiredo-Filho, L.C.S.; Iniesta, J.; Banks, C.E.; Fatibello-Filho, O. Imparting improvements in electrochemical sensors: Evaluation of different carbon blacks that give rise to significant improvement in the performance of electroanalytical sensing platforms. *Electrochim. Acta* **2015**, *157*, 125–133. [CrossRef]
53. Kariuki, J.K. An electrochemical and spectroscopic characterisation of pencil graphite electrodes. *J. Electrochem. Soc.* **2012**, *159*, H747–H751. [CrossRef]

54. King, D.; Friend, J.; Kariuki, J.K. Measuring vitamin C content of commercial orange juice using a pencil lead electrode. *J. Chem. Ed.* **2010**, *87*, 507–509. [CrossRef]
55. Ji, X.; Banks, C.E.; Crossley, A.; Compton, R.G. Oxygenated Edge Plane Sites Slow the Electron Transfer of the Ferro-/Ferricyanide Redox Couple at Graphite Electrodes. *Chem. Phys. Chem.* **2006**, *7*, 1337–1344. [CrossRef]
56. Grimaldi, A.; Heijo, G.; Mendez, E. A Multiple Evaluation Approach of Commercially Available Screen-Printed Nanostructured Carbon Electrodes. *Electroanalysis* **2014**, *26*, 1684–1693. [CrossRef]
57. Wilke, N.; Baruzzi, A.M. Comparative analysis of the charge transfer processes of the $[Ru(NH_3)_6]^{3+}/[Ru(NH_3)_6]^{2+}$ and $[Fe(CN)_6]^{3-}/[Fe(CN)_6]^{4-}$ redox couples on glassy carbon electrodes modified by different lipid layers. *J. Electroanal. Chem.* **2002**, *537*, 67–77. [CrossRef]
58. Streeter, I.; Wildgoose, G.G.; Shao, L.; Compton, R.G. Cyclic voltammetry on electrode surfaces covered with porous layers: An analysis of electron transfer kinetics at single-walled carbon nanotube modified electrodes. *Sens. Actuators B Chem.* **2008**, *133*, 462–466. [CrossRef]
59. Figueiredo-Filho, L.C.S.; Brownson, D.A.C.; Gomez-Mingot, M.; Iniesta, J.; Fatibello-Filho, O.; Banks, C.E. Exploring the electrochemical performance of graphitic paste electrodes: Graphene vs. graphite. *Analyst* **2013**, *138*, 6354. [CrossRef]
60. Nayak, P.; Kurra, N.; Xia, C.; Alshareef, H.N. Highly Efficient Laser Scribed Graphene Electrodes for On-Chip Electrochemical Sensing Applications. *Adv. Electron. Mater.* **2016**, *2*, 1600185. [CrossRef]
61. Kadara, R.O.; Jenkinson, N.; Li, B.; Church, K.H.; Banks, C.E. Manufacturing electrochemical platforms: Direct-write dispensing versus screen printing. *Electrochem. Comm.* **2008**, *10*, 1517–1519. [CrossRef]
62. Ferro, S.; De Battisti, A. Electron transfer reactions at conductive diamond electrodes. *Electrochim. Acta* **2002**, *47*, 1641–1649. [CrossRef]
63. Brownson, D.A.C.; Munro, L.J.; Kampouris, D.K.; Banks, C.E. Electrochemistry of Graphene; not such a beneficial electrode material? *RSC Adv.* **2011**, *1*, 978–988. [CrossRef]
64. Van den Beld, W.T.E.; Odijk, M.; Vervuurt, R.H.J.; Weber, J.W.; Bol, A.A.; van den Berg, A.; Eijkel, J.C.T. In Situ Raman Spectroscopy to Elucidate the Influence of Adsorption in Graphene Electrochemistry. *Sci. Reps.* **2017**, *7*, 45080. [CrossRef] [PubMed]
65. Nolan, H.; McEvoy, N.; Keeley, G.P.; Callaghan, S.D.; McGuinness, C.; Duesberg, G.S. Nitrogen-doped pyrolytic carbon films as highly electrochemically active electrodes. *Phys. Chem. Chem. Phys.* **2013**, *15*, 18688. [CrossRef]
66. Keeley, G.P.; McEvoy, N.; Kumar, S.; Peltekis, N.; Mausser, M.; Duesberg, G.S. Thin film pyrolytic carbon electrodes: A new class of carbon electrode for electroanalytical sensing applications. *Electrochem. Comm.* **2010**, *12*, 1034–1036. [CrossRef]
67. Kampouris, D.K.; Banks, C.E. Exploring the physicoelectrochemical properties of graphene. *Chem. Commun.* **2010**, *46*, 8986–8988. [CrossRef]
68. Metters, J.P.; Banks, C.E. *Nanosensors for Chemical and Biological Applications. Sensing with Nanotubes, Nanowires and Nanoparticles*; Woodhead Publishing Ltd.: London, UK, 2014.
69. Randviir, E.P.; Brownson, D.A.C.; Gomez-Mingot, M.; Kampouris, D.K.; Iniesta, J.; Banks, C.E. Electrochemistry of Q-Graphene. *Nanoscale* **2012**, *4*, 6470–6480. [CrossRef]
70. Keeley, G.P.; McEvoy, N.; Nolan, H.; Hozinger, M.; Cosnier, S.; Duesberg, G.S. Electroanalytical Sensing Properties of Pristine and Functionalized Multilayer Graphene. *Chem. Mater.* **2014**, *26*, 1807–1812. [CrossRef]
71. Brownson, D.A.C.; Varey, S.A.; Hussain, F.; Haigh, S.J.; Banks, C.E. Electrochemical properties of CVD grown pristine graphene; monolayer vs. quasi graphene. *Nanoscale* **2014**, *6*, 1607–1621. [CrossRef]
72. Lounasvuori, M.M.; Rosillo-Lopez, M.; Salzmann, C.G.; Caruna, D.J.; Holt, K.B. Electrochemical characterisation of graphene nanoflakes with functional edges. *Faraday Discuss.* **2014**, *172*, 293–310. [CrossRef]
73. Prado Tavares, P.H.C.; Sanches Barbeira, P.J. Influence of pencil lead hardness on voltammetric response of graphite reinforcement carbon electrodes. *J. Appl. Electrochem.* **2008**, *38*, 827–832. [CrossRef]
74. Feeney, R.; Kounaves, S.P. Determination of heterogeneous electron transfer rate constants at microfabricated iridium electrodes. *Electrochem. Comm.* **1999**, *1*, 453–458. [CrossRef]
75. Bond, A.M.; Mashkina, E.A.; Simonov, A.N. Critical Review of the Methods Available for Quantitative Evaluation of Electrode Kinetics at Stationary Macrodisk Electrodes. In *Developments in Electrochemistry Science Inspired by Martin Fleischmann*; Pletcher, D., Tian, Z.-Q., Williams, D.E., Eds.; John Wiley and Sons: Chichester, UK, 2014; Chapter 2. [CrossRef]
76. Sanchez-Amaya, M.; Bárcena-Soto, M.; Antaño-Lópe, R.; Rodríguez-Lópe, A.Z.; Angel Barragan, J.; Gutierrez-Becerra, A.; Roxana Larios-Durán, E. Effect of Wide Ranges of Polarization and Concentration on the Behavior of Ferricyanide/Ferrocyanide Systems Studied Through Electrochemical Measurements. *Int. J. Electrochem. Sci.* **2022**, *17*, 22016. [CrossRef]
77. Huang, B.; Myint, K.H.; Wang, Y.; Zhang, Y.; Rao, R.R.; Sun, J.; Muy, S.; Katayama, Y.; Garcia, J.C.; Fraggedakis, D.; et al. Cation-dependent Interfacial Structures and Kinetics for Outer Sphere Electron Transfer Reactions. *J. Phys. Chem. C* **2021**, *125*, 4397. [CrossRef]
78. Dumitrescu, I.; Unwin, P.R.; Macpherson, J.V. Electrochemistry at carbon nanotubes: Perspective and issues. *Chem. Commun.* **2009**, 6886–6901. [CrossRef]
79. Cassidy, J.; Howard, E.; Ronane, M.A.; O'Gorman, J. A Note on the Electrochemistry of Ferrocene Carboxylate. *Electrochem. Comm.* **1999**, *1/2*, 69–71. [CrossRef]
80. Albery, J. *Electrode Kinetics*; Clarendon Press: Oxford, UK, 1976; p. 117.

81. Nicholson, R.S. Theory and Application of Cyclic Voltammetry for Measurement of Electrode Reaction Kinetics. *Anal. Chem.* **1965**, *37*, 1351–1355. [CrossRef]
82. Lavagnini, I.; Auliochia, R.; Magno, F. An extended method for the practical evaluation of the standard rate constant from cyclic voltammetric data. *Electroanalysis* **2004**, *16*, 505–506. [CrossRef]
83. Swaddle, T.W. Homogeneous versus Heterogeneous Self-Exchange Electron Transfer Reactions of Metal Complexes: Insights from Pressure Effects. *Chem. Rev.* **2005**, *105*, 2573–2608. [CrossRef]
84. Rooney, M.B.; Coomber, D.C.; Bond, A.M. Achievement of Near-Reversible Behavior for the $[Fe(CN)_6]^{3-/4-}$ Redox Couple Using Cyclic Voltammetry at Glassy Carbon, Gold, and Platinum Macrodisk Electrodes in the Absence of Added Supporting Electrolyte. *Anal. Chem.* **2000**, *72*, 3486–3491. [CrossRef]
85. Simonov, A.N.; Morris, G.P.; Mashkina, E.A.; Bethwaite, B.; Gillow, K.; Baker, R.; Gavaghan, D.J.; Bond, A.M. Inappropriate Use of the Quasi-Reversible Electrode Kinetic Model in Simulation-Experiment Comparisons of Voltammetric Processes That Approach the Reversible Limit. *Anal. Chem.* **2014**, *86*, 8408–8417. [CrossRef]
86. Fletcher, S.; Varley, T.S. Beyond the Butler–Volmer equation. Curved Tafel slopes from steady-state current–voltage curves. *Phys. Chem. Chem. Phys.* **2011**, *13*, 5359–5364. [CrossRef] [PubMed]
87. Morris, G.P.; Simanov, A.N.; Mashkina, E.A.; Bordas, R.; Gillow, K.; Baker, R.E.; Gavaghan, D.J.; Bond, A.M. A comparison of fully automated methods of data analysis and computer assisted heuristic methods in an electrode kinetic study of pathologically variable $[Fe(CN)_6]]^{3-/4-}$ process by AC voltammetry. *Anal. Chem.* **2013**, *85*, 11780–11787. [CrossRef] [PubMed]
88. Robinson, M.; Simonov, A.N.; Zhang, J.; Bond, A.M.; Gavaghan, D. Separating the Effects of Experimental Noise from Inherent Systemility in Voltammetry: The $[Fe(CN)_6]^{3-/4-}$ Process. *Anal. Chem.* **2019**, *91*, 1944–1953. [CrossRef]
89. Gundry, L.; Kennedy, G.; Keith, J.; Robinson, M.; Gavaghan, D.; Bond, A.M.; Zhang, J. A Comparison of Bayesian Inference Strategies for Parameterisation of Large Amplitude AC Voltammetry Derived from Total Current and Fourier Transformed Versions. *ChemElectroChem* **2021**, *8*, 2238–2258. [CrossRef]
90. Gavaghan, D.J.; Cooper, J.; Daly, A.C.; Gill, C.; Gillow, K.; Robinson, M.; Simonov, A.N.; Zhang, J.; Bond, A.M. Use of Bayesian Inference for Parameter Recovery in DC and AC Voltammetry. *ChemElectroChem* **2018**, *5*, 917–935. [CrossRef]
91. Intan, N.N.; Pfaendtner, J. Composition of Oxygen Functional Groups on Graphite Surfaces. *J. Phys. Chem. C* **2022**, *126*, 10653–10667. [CrossRef]
92. McDermott, C.A.; Kneten, K.R.; McCreery, R.L. Electron Transfer Kinetics of Aquated $Fe^{3+/2+}$, $Eu^{3+/2+}$ and $V^{3+/2+}$ at Carbon Electrodes: Inner Sphere Catalysis by Surface Oxides. *J. Electrochem. Soc.* **1993**, *140*, 2593–2599. [CrossRef]
93. Lu, Y.; Li, X.; Compton, R.G. Oxygen Reduction Reaction at Single Entity Multiwalled Carbon Nanotubes. *J. Phys. Chem. Letts.* **2022**, *13*, 3748–3753. [CrossRef]
94. Banks, C.E.; Ji, X.; Crossley, A.; Compton, R.G. Understanding the Electrochemical Reactivity of Bamboo Multiwalled Carbon Nanotubes: The Presence of Oxygenated Species at Tube Ends May not Increase Electron Transfer Kinetics. *Electroanalysis* **2006**, *18*, 2137–2140. [CrossRef]
95. Chou, A.; Böcking, T.; Singh, N.K.; Gooding, J.J. Demonstration of the importance of oxygenated species at the ends of carbon nanotubes for their favourable electrochemical properties. *Chem. Commun.* **2005**, 842–844. [CrossRef]
96. Lai, S.C.; Patel, A.N.; McKelvey, K.; Unwin, P.R. Definitive Evidence for Fast Electron Transfer at Pristine Basal Plane Graphite from High-Resolution Electrochemical Imaging. *Angew. Chem. Int. Ed.* **2012**, *51*, 5405–5408. [CrossRef] [PubMed]
97. Velický, M.; Toth, P.S.; Woods, C.; Novoselov, K.S.; Dryfe, R.A.W. Electrochemistry of the Basal Plane versus Edge Plane of Graphite Revisited. *J. Phys. Chem. C* **2019**, *123*, 11677–11685. [CrossRef]
98. Banks, C.E.; Davies, T.J.; Wildgoose, G.G.; Compton, R.G. Electrocatalysis at Graphite and Carbon Nanotube Modified Electrodes: Edge-Plane Sites and Tube Ends Are the Reactive Sites. *Chem. Commun.* **2005**, 829–841. [CrossRef] [PubMed]
99. Rice, R.J.; McCreery, R.L. Quantitative Relationship between Electron Transfer Rate and Surface Microstructure of Laser-Modified Graphite Electrodes. *Anal. Chem.* **1989**, *61*, 1637–1641. [CrossRef]
100. Unwin, P.R.; Guell, A.G.; Zhang, G. Nanoscale Electrochemistry of sp^2 Carbon Materials: From Graphite and Graphene to Carbon Nanotubes. *Acc. Chem. Res.* **2016**, *49*, 2041–2048. [CrossRef]
101. Premkumar, J.; Khoo, S.B. Electrocatalytic oxidations of biological molecules (ascorbic acid and uric acids) at highly oxidized electrodes. *J. Electroanal. Chem.* **2005**, *576*, 105–112. [CrossRef]
102. Noel, M.; Anantharaman, P.N. Voltammetric Studies on a Glassy Carbon Electrode Part II Factors Influencing the Simple Electron-transfer Reactions–the $K_3[Fe(CN)_6]$ – K_4 $[Fe(CN)_6]$ System. *Analyst* **1985**, *110*, 1095–1103. [CrossRef]
103. Lee, S.J.; Theerthagiri, J.; Nithyadharseni, P.; Arunachalam, P.; Balaji, D.; Kumar, A.M.; Madhavan, J.; Mittal, V.; Choi, M.Y. Heteroatom-doped graphene-based materials for sustainable energy applications: A review. *Renew. Sustain. Energy Rev.* **2021**, *143*, 110849. [CrossRef]
104. Brownson, D.A.C.; Banks, C.E. *The Handbook of Graphene Electrochemistry*; Springer: Berlin/Heidelberg, Germany, 2014; Chapters 1,3.
105. Brownson, D.A.C.; Kampouris, D.K.; Banks, C.E. Graphene electrochemistry: Fundamental concepts through to prominent applications. *Chem. Soc. Rev.* **2012**, *41*, 6944–6976. [CrossRef]
106. Punckt, C.; Pope, M.A.; Liu, J.; Lin, Y.; Aksay, I.A. Electrochemical Performance of Graphene as Effected by Electrode Porosity and Graphene Functionalization. *Electroanalysis* **2010**, *22*, 2834–2841. [CrossRef]
107. Wang, J.; Yang, S.; Guo, D.; Yu, P.; Li, D.; Ye, J.; Mao, L. Comparative studies on electrochemical activity of graphene nanosheets and carbon nanotubes. *Electrochem. Comms.* **2009**, *11*, 1892–1895. [CrossRef]

108. Shang, N.G.; Papakonstantinou, P.; McMullan, M.; Chu, M.; Stamboulis, A.; Potenza, A.; Dhesi, S.S.; Marchetto, H. Catalyst-Free Efficient Growth, Orientation and Biosensing Properties of Multilayer Graphene Nanoflake Films with Sharp Edge Planes. *Adv. Funct. Mater.* **2008**, *18*, 3506–3514. [CrossRef]
109. Tang, L.; Wang, Y.; Li, Y.; Feng, H.; Lu, J.; Li, J. Preparation, Structure, and Electrochemical Properties of Reduced Graphene Sheet Films. *Adv. Funct. Mater.* **2009**, *19*, 2782–2789. [CrossRef]
110. Lounasvuori, M.M.; Rosillo-Lopez, M.; Salzmann, C.; Caruana, D.J.; Holt, K.B. The influence of acidic edge groups on the electrochemical performance of graphene nanoflakes. *J. Electroanal. Chem.* **2015**, *753*, 28–34. [CrossRef]
111. Patel, A.N.; Guille Collignon, M.; O'Connell, M.A.; Hung, W.O.Y.; McKelvey, K.; Macpherson, J.V.; Unwin, P.R. A New View of Electrochemistry at Highly Oriented Pyrolytic Graphite. *J. Am. Chem. Soc.* **2012**, *134*, 20117–20130. [CrossRef] [PubMed]
112. Beriet, C.; Pletcher, D. A microelectrode study of the mechanism and kinetics of the ferro/ferricyanide couple in aqueous media: The influence of the electrolyte and its concentration. *J. Electroanal. Chem.* **1993**, *361*, 93–101. [CrossRef]
113. Kůta, J.; Yeager, E. The influence of cations on the electrode kinetics of ferricyanide-ferrocyanide system on the rotating gold electrode. *J. Electroanal. Chem. Interfacial. Electrochem.* **1975**, *59*, 110–112. [CrossRef]
114. Bindra, P.; Gerischer, H.; Peter, L.M. The dependence of the rate of the $Fe(CN)_6^{3-}/Fe(CN)_6^{4-}$ couple on ionic strength in concentrated solutions. *J. Electroanal. Chem. Interfacial. Electrochem.* **1974**, *57*, 435–438. [CrossRef]
115. Campbell, S.A.; Peter, L.M. The effect of $[K^+]$ on the heterogeneous rate constant for the $[Fe(CN)_6]^{3-}/[Fe(CN)_6]^{4-}$ redox couple investigated by a.c. impedance spectroscope. *J. Electroanal. Chem.* **1994**, *364*, 257–260. [CrossRef]
116. Kawiak, J.; Kulesza, P.J.; Galus, Z. A search for conditions permitting model behavior of the $Fe(CN)_6^{3-/4-}$ system. *J. Electroanal. Chem. Interfacial. Electrochem* **1987**, *226*, 305–314. [CrossRef]
117. Goldstein, E.L.; Van de Mark, M.R. Electrode cleaning and anion effects on k_s for $K_3Fe(CN)_6$ couple. *Electrochim. Acta* **1982**, *27*, 1079–1085. [CrossRef]
118. Kim, D.Y.; Wang, J.; Yang, J.; Kim, H.W.; Swain, G.M. Electrolyte and Temperature Effects on the Electron Transfer Kinetics of $Fe(CN)_6^{-3/-4}$ at Boron-Doped Diamond Thin Film Electrodes. *J. Phys. Chem. C* **2011**, *115*, 10026–10032. [CrossRef]
119. McLean, J.D.; Timnick, A. Frumkin Double-Layer Corrections Applied to the Heterogeneous Rate Constants for Cd(ll) Evaluated by Alternating Current Polarography. *Anal. Chem.* **1967**, *39*, 1669–1671. [CrossRef]
120. Schrattenecker, J.D.; Heer, R.; Melnik, E.; Maier, T.; Fafilek, G.; Hainberger, R. Hexaammineruthenium (II)/(III) as alternative redox-probe to Hexacyanoferrate (II)/(III) for stable impedimetric biosensing with gold electrodes. *Biosens. Bioelect.* **2019**, *127*, 25–30. [CrossRef]
121. Lazar, J.; Schnelting, C.; Slavcheva, E.; Schnakenberg, U. Hampering of the Stability of Gold Electrodes by Ferri-/Ferrocyanide Redox Couple Electrolytes during Electrochemical Impedance Spectroscopy. *Anal. Chem.* **2016**, *88*, 682–687. [CrossRef]
122. Dijksma, M.; Boukamp, B.A.; Kamp, B.; van Bennekom, W.P. Effect of Hexacyanoferrate(II/III) on Self-Assembled Monolayers of Thioctic Acid and 11-Mercaptoundecanoic Acid on Gold. *Langmuir* **2002**, *18*, 3105–3112. [CrossRef]
123. Hua, X.; Xia, H.-L.; Long, Y.-T. Revisiting a classical redox process on a gold electrode by operando ToF-SIMS: Where does the gold go? *Chem. Sci.* **2019**, *10*, 6215–6219. [CrossRef]
124. Fleischmann, M.; Graves, P.R.; Robinson, J. The raman spectroscopy of the ferricyanide/ferrocyanide system at gold, β-palladium hydride and platinum electrodes. *J. Electroanal. Chem. Interf. Electrochem.* **1985**, *182*, 87–98. [CrossRef]
125. Korzeniewski, C.; Severson, V.M.W.; Schmidt, P.P.; Pons, S.; Fleischmann, M. Theoretical Analysis of the Vibrational Spectra of Ferricyanide and Ferrocyanide Adsorbed on Metal Electrodes. *J. Phys. Chem.* **1987**, *91*, 5568–5573. [CrossRef]
126. Kulesza, P.; Jędral, T.; Galus, Z. The electrode kinetics of the $Fe(CN)_6^{3-}/Fe(CN)_6^{4-}$ system on the platinum rotating electrode in the presence of different anions. *J. Electroanal. Chem. Interf. Electrochem.* **1980**, *108*, 141–149. [CrossRef]
127. Dourado, A.H.B. Review Electric Double Layer: The Good, the Bad, and the Beauty. *Electrochem* **2022**, *3*, 789–808. [CrossRef]
128. Jenkins, H.D.B.; Thakur, K.P. Reappraisal of Thermochemical Radii for Complex Ions. *J. Chem. Ed.* **1979**, *56*, 576–577. [CrossRef]
129. Kneten, K.R.; McCreery, R.L. Effects of redox system structure on electron transfer kinetics at ordered graphite and glassy carbon electrodes. *Anal. Chem.* **1992**, *64*, 2518–2524.
130. Pumera, M. Electrochemistry of graphene, graphene oxide and other graphenoids: Review. *Electrochem. Comm.* **2013**, *36*, 14–18. [CrossRef]
131. Tan, C.; Rodríguez-López, J.; Parks, J.J.; Ritzert, N.L.; Ralph, D.C.; Abruna, H.D. Reactivity of Monolayer Chemical Vapor Deposited Graphene Imperfections Studied Using Scanning Electrochemical Microscopy. *ACS Nano* **2012**, *6*, 3070–3079. [CrossRef]
132. McDermott, M.T.; Kneten, K.; McCreery, R. Anthraquino-nedisulfonate Adsorption, Electron-Transfer Kinetics, and Capacitance on Ordered Graphite Electrodes: The Important Role of Surface Defects. *J. Phys. Chem.* **1992**, *96*, 3124–3130. [CrossRef]
133. Dong, J.; Sheng, Z.; Xue, G. Fourier Transform Surface Enhanced Raman Scattering Study of Ferricyanide on Silver. *Spectros. Letts.* **1995**, *28*, 139–151. [CrossRef]
134. Datta, M.; Datta, A. In situ FTIR and XPS studies of hexacyanoferrate redox systems. *J. Phys. Chem.* **1990**, *94*, 8203–8207. [CrossRef]
135. Pharr, C.M.; Griffiths, P.R. Infrared Spectroelectrochemical Analysis of Adsorbed Hexacyanoferrate Species Formed during Potential Cycling in the Ferrocyanide/Ferricyanide Redox Couple. *Anal. Chem.* **1997**, *69*, 4673–4679. [CrossRef]
136. Ganesan, A.; Zimudzi, T.J.; Pothanamkandathi, V.; Gorski, C.A.; Hall, D.M. Spectroelectrochemical Examination of the Ferro-Ferricyanide Redox Reaction: Impacts of Electrode Thickness and Applied Potential. *J. Electrochem. Soc.* **2022**, *169*, 106501. [CrossRef]

137. Piechota, E.J.; Meyer, G.J. Introduction to Electron Transfer: Theoretical Foundations and Pedagogical Examples. *J. Chem. Educ.* **2019**, *96*, 2450–2466. [CrossRef]
138. Krejci, J.; Sajdlova, Z.; Nedela, V.; Flodrova, E.; Sejnohova, R.; Vranova, H.; Plicka, R. Effective Surface Area of Electrochemical Sensors. *J. Electrochem. Soc.* **2014**, *161*, B147–B150. [CrossRef]
139. De Carvalho, R.C.; Betts, A.J.; Cassidy, J.F. Sodium diclofenac determination using CeO_2 nanoparticle modified screenprinted electrodes—A study of background correction. *Microchem. J.* **2020**, *158*, 105258. [CrossRef]
140. Ahmad, K.; Kumara, P.; Mobin, S.M. A highly sensitive and selective hydroquinone, sensor based on a newly designed N-rGO/$SrZrO_3$ composite. *Nanoscale. Adv.* **2020**, *2*, 502–511. [CrossRef] [PubMed]
141. Coelho, D.; Luiz, G.M.; Machado, S.A.S. Estimating the Electrochemically Active Area: Revisiting a Basic Concept in Electrochemistry. *J. Braz. Chem. Soc.* **2021**, *32*, 1912–1917. [CrossRef]
142. Killedar, L.S.; Shanbhag, M.M.; Shetti, N.P.; Malode, S.J.; Veerapur, R.S.; Reddy, K.R. Novel graphene-nanoclay hybrid electrodes for electrochemical determination of theophylline. *Microchem. J.* **2021**, *165*, 106115. [CrossRef]
143. Mariyappan, V.; Karuppusamy, N.; Chen, S.-M.; Raja, P.; Ramachandran, P. Electrochemical determination of quercetin using glassy carbon electrode modified with WS2/$GdCoO_3$ nanocomposite. *Microchim. Acta* **2022**, *189*, 118. [CrossRef]
144. Zhao, Y.; Nakamura, R.; Kamiya, K.; Nakanishi, S.; Hashimoto, K. Nitrogen-doped carbon nanomaterials as non-metal electrocatalysts for water oxidation. *Nat. Comms.* **2013**, *4*, 2390. [CrossRef]
145. Savéant, J.-M.; Tessier, D. Variation of the Electrochemical Transfer Coefficient with Potential. *Faraday Discuss. Chem. Soc.* **1982**, *74*, 57–72. [CrossRef]
146. Watson, D.F.; Bocarsly, A.B. The effects of electronic coupling and solvent broadening on the intervalent electron transfer of a centrosymmetric mixed-valence complex. *Coord. Chem. Revs.* **2001**, *211*, 177–194. [CrossRef]
147. Seri, O. Kinetic parameter determination of ferri/ferrocyanide redox reaction using differentiating polarization curve technique. *Electrochim. Acta* **2019**, *323*, 134776. [CrossRef]
148. Khadke, P.; Tichter, T.; Boettcher, T.; Muench, F.; Ensinger, W.; Roth, C. A simple and effective method for the accurate extraction of kinetic parameters using differential Tafel plots. *Sci. Reps.* **2021**, *11*, 8974. [CrossRef] [PubMed]
149. Fletcher, S. Tafel slopes from first principles. *J. Solid State Electrochem.* **2009**, *13*, 537–549. [CrossRef]
150. Savéant, J.-M. Effect of Ion Pairing on the Mechanism and Rate of Electron Transfer. Electrochemical Aspects. *J. Phys. Chem. B* **2001**, *105*, 8995–9001. [CrossRef]
151. Zhen, F.; Percevault, L.; Paquin, L.; Limantion, E.; Lagrost, C.; Hapiot, P. Electron Transfer Kinetics in a Deep Eutectic Solvent. *J. Phys. Chem. B* **2020**, *124*, 1025–1032. [CrossRef] [PubMed]
152. Frenzel, N.; Hartley, J.; Frisch, G. Voltammetric and spectroscopic study of ferrocene and hexacyanoferrate and the suitability of their redox couples as internal standards in ionic liquids. *Phys. Chem. Chem. Phys.* **2017**, *19*, 28841–28852. [CrossRef]
153. Iamprasertkun, P.; Ejigu, A.; Dryfe, R.A.W. Understanding the electrochemistry of "water-insalt" electrolytes: Basal plane highly ordered pyrolytic graphite as a model system. *Chem. Sci.* **2020**, *11*, 6978–6989. [CrossRef]
154. Peter, L.M.; Dürr, W.; Bindra, P.; Gerischer, H. The influence of alkali metal cations on the rate of the ferrocyanide/ferricyanide electrode processes. *J. Electroanal. Chem. Interfacial Electrochem.* **1976**, *71*, 31–50. [CrossRef]